University of Nevada, Reno

A Scoping Study to Develop a Computational Fluid Dynamics Based Model to Predict Radiological Materials Packaging Temperatures within a Generic Staging Building

A thesis submitted in partial fulfillment of the
requirements for the degree of Master of Science in
Mechanical Engineering

by

Joel A. Kaderka

Dr. Miles Greiner/Thesis Advisor

May, 2021

DOE/NV/03624--1092

THE GRADUATE SCHOOL

We recommend that the thesis
prepared under our supervision by

JOEL A. KADERKA

entitled

A Scoping Study to Develop a Computational Fluid Dynamics Based Model to Predict Radiological Materials Packaging Temperatures within a Generic Staging Building

be accepted in partial fulfillment of the
requirements for the degree of

MASTER OF SCIENCE

Miles Greiner, Ph.D.
Advisor

Mustafa Hadj-Nacer, Ph.D.
Co-advisor

Aditya Nair, Ph.D.
Committee Member

Sage Hiibel, Ph.D.
Graduate School Representative

David W. Zeh, Ph.D., Dean
Graduate School

May, 2021

Abstract

The objective of this work is to perform computational fluid dynamics simulations of a ventilated radiological-material-package staging building to determine the effect of including or excluding a variety of physical effects and computational methods on both the predicted package temperatures and required computational resources. The generic building contains 640 drum-packages containing heat-generating, radiological material supported on four racks that are eight levels tall. Additionally, there is a forced ventilation system, lighting, and insulated walls. Computational models were constructed that included or excluded (a) shelving, (b) effects of unsteadiness, and (c) radiation heat transfer. Simulations with each drum modeled separately were compared to simpler simulations with sets of four drums represented by an equivalent box-package. These models employed between 10^6 to 10^7 elements.

Steady state simulations predicted package temperatures that were within 0.1°C of simulations that included transient effects and required only one-eighth the computational resources. Calculations that excluded shelving predicted temperatures within 0.6°C of simulations that included shelving and required one-fourth the computational resources. Excluding radiation heat transfer systematically increased temperatures by around 1.5°C but reduced computational resources by a factor of four. The box-package model reduced the computational resources by a factor of 3, but systematically predicted higher temperatures by around 1.1°C. These results will be used to develop an efficient computational fluid dynamics model to assess the ability of different staging building designs to prevent the temperature of package components from exceeding specified limits.

Acknowledgements

First, I would like to thank my advisors Dr. Miles Greiner and Dr. Mustafa Hadj Nacer for their guidance, teaching, and support. They have helped me learn software and general research procedures which I plan to use throughout my engineering career and have helped me make connections throughout the aerospace industry. This work would not have been possible without them. I would also like to thank Dr. Aditya Nair and Dr. Sage Hiibel for being members of my thesis committee.

I would like to thank my parents, John and Paula Kaderka, and brother, Jeremy Kaderka for their love and support. Without their continuous support, “care packages”, and ideas to investigate, I would not be where I am today.

I would like to thank my friends, namely: Andrew Morgan, Bruno Reyes, Dan Carey, Greg Turri, Jose Carrillo, Justin Siao, Kegan Rahe, M Iffat Hassan, Megan Higley, Michael Segura, Mitch Lane, Skyler Russ, Tyler Hinson, and Will Crain. I am thankful to have their friendship and late-night distractions over the years.

Lastly, I would like to thank my girlfriend Sarah Cronk, whose brilliant mind, patience, understanding, proofreading, and support have been a tremendous help. I hope to be as supportive for her throughout her pursuance of a Doctorate in Physical Therapy.

There are many more whose friendship and guidance I am deeply thankful for.

This work was supported by Mission Support and Test Services, LLC, under Contract No. DE-NA0003624 with the U.S. Department of Energy

Table of Contents

List of Tables

List of Figures

Nomenclature

Roman Letters

C_P	Average Specific Heat at Constant Pressure
$\dot{m}$	Mass Flow Rate
M	Molecular
N	Number of Box-packages
P	Pressure
Q	Heat Generation Rate
R	Radius or Universal Gas Constant
$\bar{T}$	Average Temperature
T	Temperature
t	Time

Greek Letters

ΔT	Temperature Difference
ϵ	Emissivity
ρ	Density
σ	Standard Error of the Estimate

Subscripts

%	Percent Difference
1L	First Law
95%	Two-Standard
A	Actual
Avg	Average
B	Box-package

D	Drum-package
G	Grid
I	Inlet
JE	Jacobs Engineering
L	Limit
Max	Maximum
OP	Operating Pressure
P	Package
R	Return
Room	Room
S	Simulated
SM	Safety Margin
T	Theoretical
W	Weight

Acronyms

3D	Three-Dimensional
AL	Aluminum
CFD	Computational Fluid Dynamics
CFL	Courant Friedrichs Lewey Stability Criteria
EXT	External
GPU	Graphics Processing Unit
HAC	Hypothetical Accident Conditions
HVAC	Heating, Ventilation, and Air Conditioning
JE	Jacobs Engineering
LES	Large Eddy Simulation

L	Extra-Low Carbon
NCT	Normal Conditions of Transport
PCV	Primary Containment Vessel
PLCS	Places
Rad	Radiation Heat Transfer
RNG k-ε	Renormalization Group, Turbulent Kinetic Energy - Turbulent Dissipation
RC	Resource Cost
SARP	Safety Analysis Report for Packaging
SCV	Secondary Containment Vessel
SS	Stainless Steel or Steady State
SST k-ω	Shear Stress Transport, Turbulent Kinetic Energy - Specific Rate of Dissipation

Chapter 1: Introduction

1.1. Background

The National Nuclear Security Administration stages radiological materials in drum-style packages. Packages that transport, store, or stage radiological materials must contain their content material, shield their surroundings from radiation, and assure that their contents are radiologically subcritical under both Normal Conditions of Transport (NCT) and a series of Hypothetical Accident Conditions (HAC) [1].

The current work examines an optimized radiological material staging building. This air-conditioned building would contain multi-level warehouse shelving with aisles to allow forklift loading of drum-style radiological materials packages. Specifically, our goal is to develop a computational fluid dynamics-based tool to predict the margin between all package component temperatures and their allowed limits for a range of package heat generation rates (up to 19W), number of packages in the building, and a range of ventilation airflow rates and inlet temperatures.

1.2. Model 9975 Radiological Materials Package

Figure 1 shows a cross section of the 9975 radiological materials package (referred to as package) [2]. The package is almost entirely axisymmetric about its central axis. The radiological contents in the package center are shown in red. They are contained in three nested 3013 Cans, made from 304L stainless-steel (SS 304L), shown in orange. The convenience can is the innermost, with an outer length of 20.9cm (8.235in), outer radius of 5.6cm (2.205in), and thickness of 0.81mm (0.032in). The next larger can is the

inner can, with an outer length of 23.1cm (9.1in), outer radius of 5.9cm (2.305in), and thickness of 1.3mm (0.05in). The outer 3013 can has an outer length of 25.4cm (10in), outer radius of 6.4cm (2.5in), and thickness of 3mm (0.118in). The outer can is held in place by an aluminum honeycomb impact absorber shown in yellow on the bottom, and a spacer sleeve shown in green on the top. The spacer sleeve is 1100 aluminum with a length of 12.4cm (4.9in), outer radius of 6.4cm (2.5in), and thickness of 3mm (0.118in). This ensures a 2.5mm (0.1in) gas-filled gap will be above the spacer sleeve. The impact absorber under the outer can sits at the bottom of the Primary Containment Vessel (PCV).

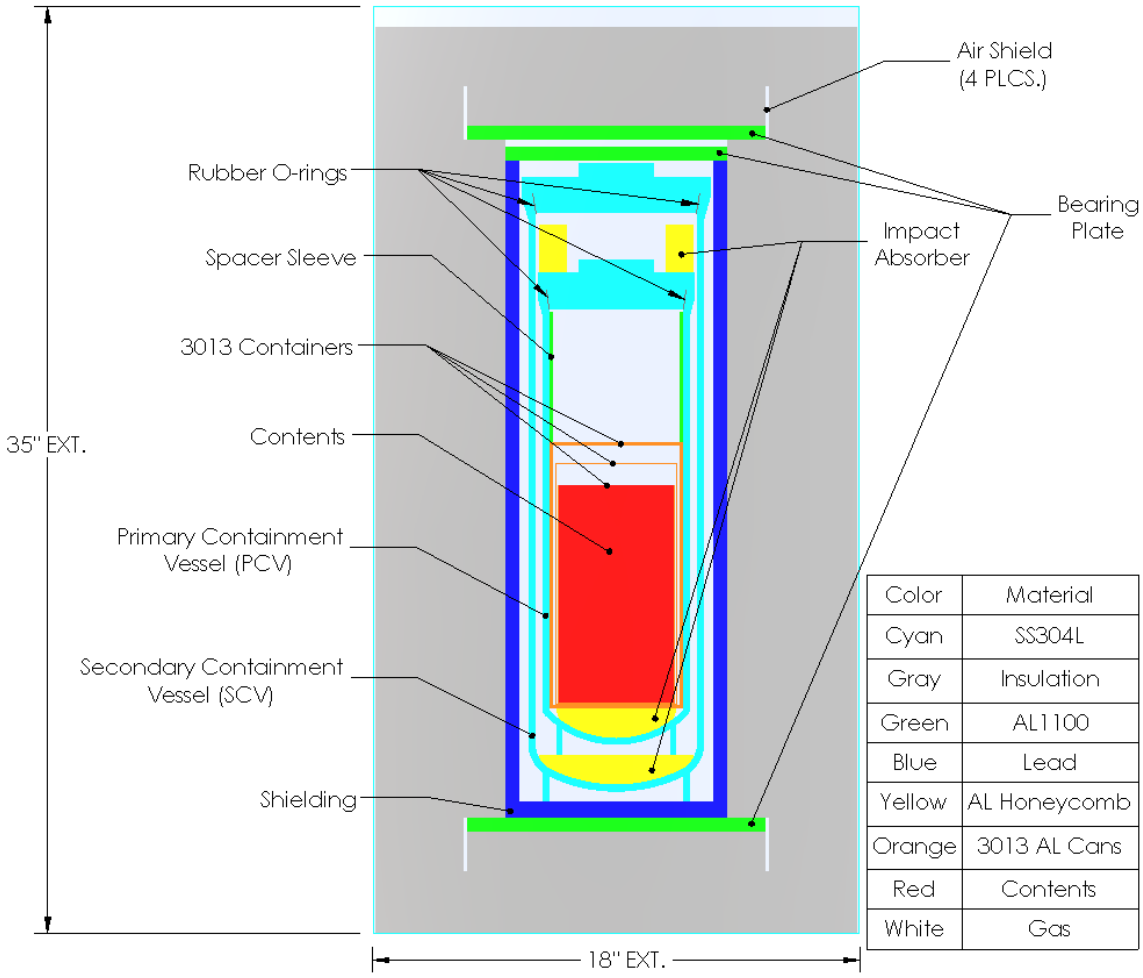

Figure 1: A cross-section of the axisymmetric 9975 package shows its components, dimensions, and materials [2].

The PCV, shown in cyan, is made of SS 304L 5”-diameter Schedule 40 tubing with a butt-joint welded cap on the bottom. A SS 304L ring base is welded to the bottom of that. The top lid is a threaded screw cap with an integrated 5.1cm (2in) square nut, which is the only non-axisymmetric component of the 9975 package. It is sealed with two rubber O-rings, whose locations are shown. These seals allow the PCV to be backfilled with an inert gas (usually helium) shown in white and then hermetically sealed. The PCV is supported by an impact absorber shown in yellow and is held in place by an impact absorber ring shown in yellow on top. The impact absorber ring has a length of 4.6cm (1.8in), outer radius of 7.4cm (2.9in), and thickness of 2.7cm (1.05in). Surrounding the PCV is the Secondary Containment Vessel (SCV) shown in cyan. It is similar to the PCV but constructed using 6”-diameter Schedule 40 SS 304L tubing. The SCV is also backfilled with an inert gas. The PCV and SCV seals provide double containment of the contents.

The bottom and sides of the SCV are surrounded by lead shown in dark blue which has an outer length of 62.7cm (24.7in), outer radius of 10.6cm (4.18in), and thicknesses of 1.5cm (0.6in) and 1.4cm (0.55in) respectively. A 1100 aluminum solid bearing plate which has a radius of 10.6cm (4.18in) and thickness of 1.3cm (0.5in) is shown in green on top. Any white gaseous region outside of the SCV is air. There is another set of 1100 aluminum solid bearing plates each with a radius of 14.2cm (5.6in) and thickness of 1.3cm (0.5in) shown in green above and below the lead. These support the lead and internal components by distributing internal loads to avoid crushing the insulative material. There are two rings of air shown in white on the end of the outermost bearing plates, known as “air shields”, which aid in thermal dissipation from the end of the bearing plates. Surrounding the lead is Celotex insulation material shown in gray. It is designed to conduct heat from the contents during NCT and protect the internal components from damage in the event of accident conditions.

The outermost component is the 35-gallon, 18-gauge (.048” thick) SS 304L drum shown in cyan which provides structure and damage protection during shipping and staging. There is an additional ring built into the drum’s bottom which acts as a stand, as well as hoops on the curved surface which provide rigidity during rolling. These are often neglected from models. This should not significantly affect the results as they are external components, and the temperature gradient in these regions is small. With these components, the package is roughly 53cm (21in) in diameter and 91cm (36in) tall [2].

Analysis and testing performed by Savannah River National Laboratory and presented in a Safety Analysis Report for Packaging (SARP) predicts package temperatures under NCT and compares those temperatures to allowed limits [2]. NCT consists of 38°C (100°F) ambient air with total insolation over a 12-hour period of 800 g cal/cm^2 on horizontal flat surfaces (excluding the base), 200 g cal/cm^2 on flat surfaces not transported horizontally, and 400 g cal/cm^2 on curved surfaces. The analysis assumes the heat generating contents produce 19W.

For each package component, Table 1 summarizes the maximum predicted NCT temperature, its allowable limit under NCT, and the safety margin between those temperatures. During NCT, the O-ring temperatures must not exceed 204°C (400°F). The metal of the PCV/SCV must not exceed 149°C (300°F), the lead shielding must not exceed 328°C (622°F) (lead’s melting point), and the insulation bulk temperature must not exceed 121°C (250°F) [2]. No temperature limit was specified for the package contents. Finally, the external drum surface must not exceed 50°C (122°F) [1]. By design, none of the predicted temperatures exceeded their specified limit and the drum surface has the smallest margin of safety.

Table 1: Each component of the 9975 package under NCT has a temperature limit, calculated maximum temperature, and a margin between allowed and calculated temperature.

Component	Temperature Limit, T_L [°F]	Calculated Maximum Temperature, T_{Max} [°F]	Safety Margin, $T_{SM} = T_L - T_{Max}$ [°F]
Contents	N/A	411	N/A
PCV O-rings	400	160	240
PCV	300	181	119
SCV O-rings	400	156	244
SCV	300	166	134
Shielding	622	156	466
Insulation	250	155	95
Drum	122	114	8

While the 9975 package component temperatures were predicted under NCT conditions, our goal is to predict component temperatures for many packages staged in a ventilated building.

1.3. Radiological Material Staging Buildings

Figure 2 is an isometric view of a potential staging building computational model constructed by Jacobs Engineering [3]. They modeled a room that is roughly 18.3m long x 9.1m wide x 9.1m tall (60ft 6in x 30ft x 29ft 6in) with adiabatic walls. There are two 71cm (28in) wide x 76cm (30in) tall indentations running the length of the long walls, whose bottoms are located 5.6m (18.5ft) from the floor. These may be support beams for the wall, but their purpose is not specified. There are both lighting and Heating, Ventilation, and Air Conditioning (HVAC) supply and return ducting near the ceiling. The building contains secure shelving with rectangular heat-generating boxes on the shelves and aisles between the shelves. Figure 2 shows that there is an open space between the racks and

the right-hand wall where the entry doors are located. Figure 3 shows three orthographic views of the model. While Jacobs Engineering did not specify the exact dimensions and materials of their model, this section describes the author's understanding and best approximation of their work.

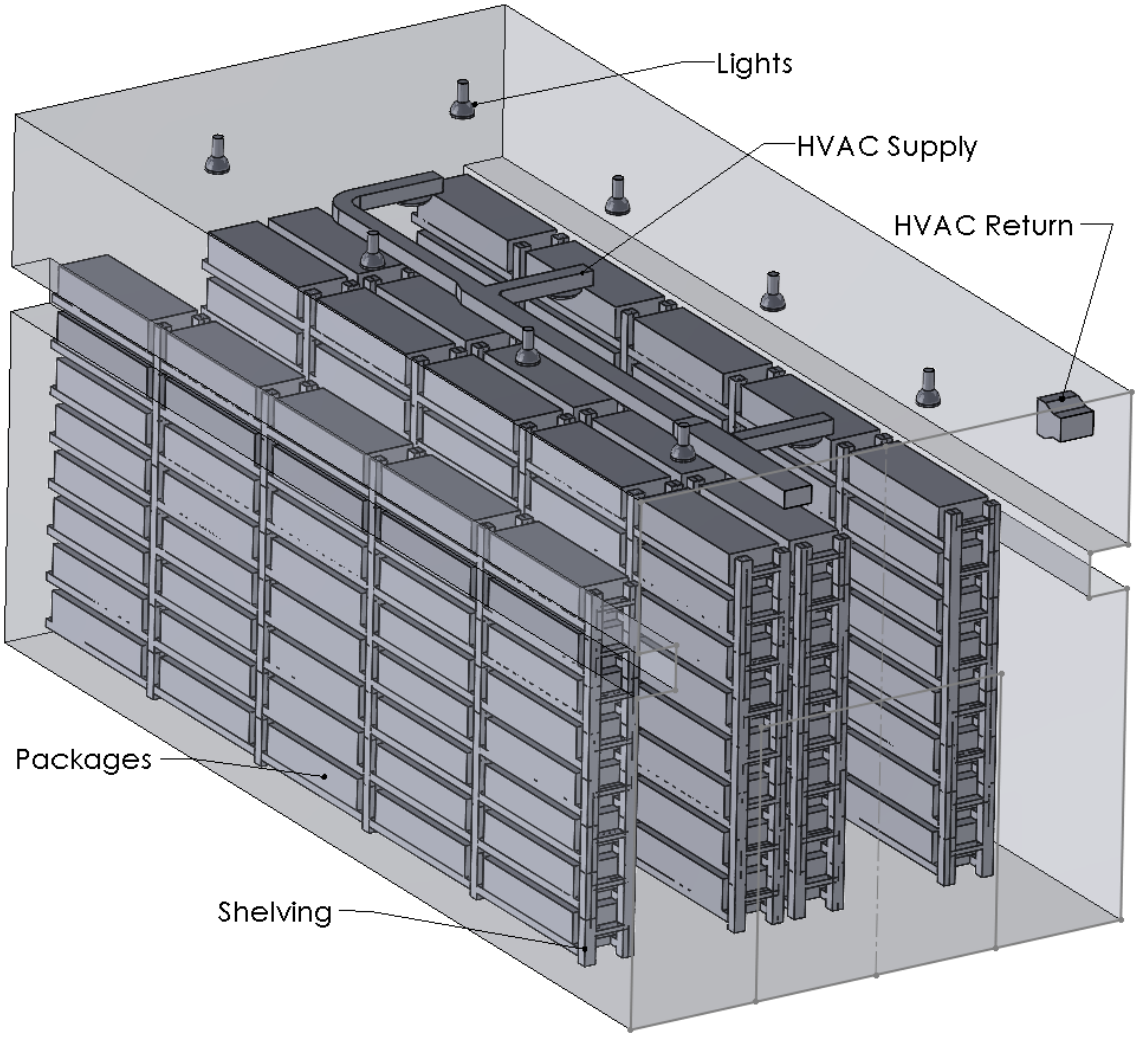

Figure 2: An isometric view of a computational model of a potential radiological material staging building includes insulated room walls, heat generating lighting, HVAC ducting, and secure shelving with rectangular heat generating boxes loaded on the shelving.

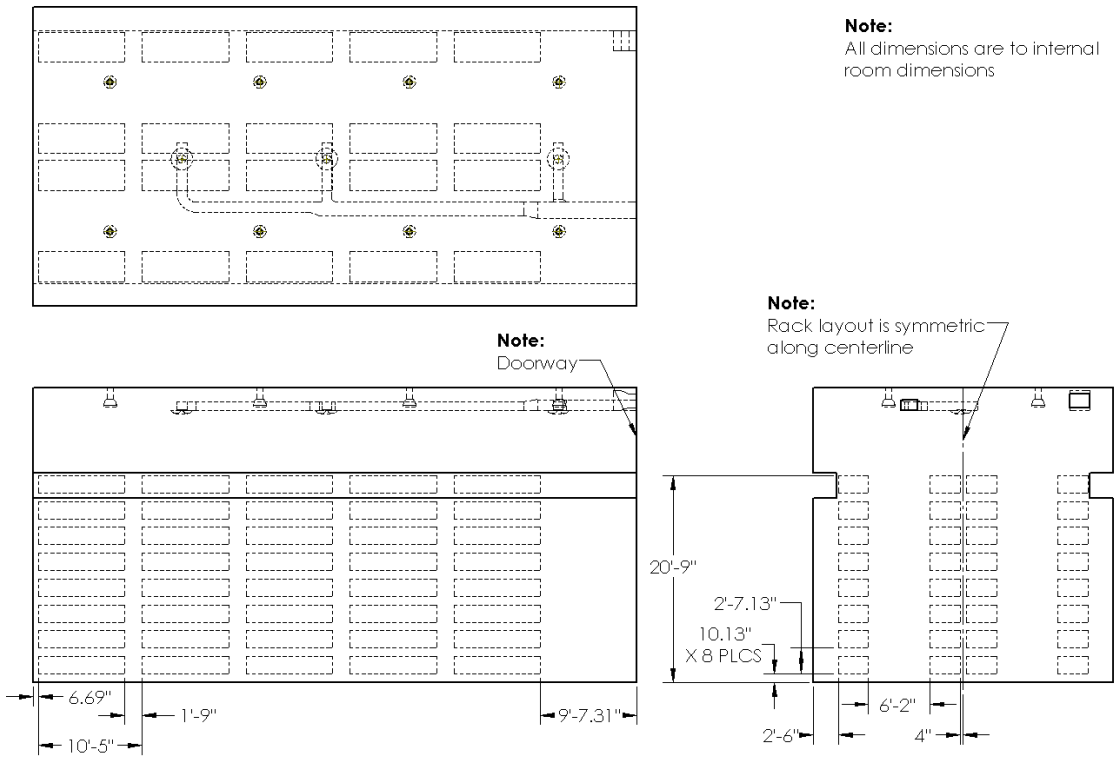

Figure 3: Three orthographic views of the computational model provide the layout of the boxes in the room. Dimensions are in inches.

The building has 8 lights generating 100W of heat each, and three HVAC diffusers near the ceiling. The HVAC system provides 0.78 kg/s (1370 ACFM) of air at 17.8°C (64°F) and allows air to freely return through one return duct.

In this model, each shelving bay holds four 9975 packages lying on their sides, with each package having an external diameter of 53cm (21in) and an external length of 91cm (36in). However, to simplify the model, instead of modeling packages individually, sets of four packages are represented by one rectangular box (referred to as box) whose length, width, and height dimensions are 264cm x 91cm x 53cm (104in x 36in x 21in), respectively. This assumption was not validated or verified by experiments or other models.

Figure 2 shows that the racking system was designed to allow four rows of racks, mounted to the left-hand wall. This allows forklift maneuverability through the entrance

door on the other end of the room. The distance from the racks to the door wall is 2.9m (9ft 7in). The two center racks are 20cm (8in) apart, allowing two 188cm (74in) wide aisles for forklift movement. There are five columns of bays on each rack, which can be stacked either eight or ten levels tall depending on the design. This represents a total of either 640 or 800 9975-cylindrical packages (160 or 200 boxes) each generating 13, 16, or 19W. The 640-package case will be examined in this work, with a total room heat generation of 9,120, 11,040, and 12,960W. The computational model had 10.3 million elements based on a mesh sensitivity study and utilized the Shear Stress Transport (SST) k-ω turbulence model [4]. Conductive heat transfer within the solid and air regions and natural and forced convection in the air regions are modeled. It is unclear if Jacobs Engineering modeled radiation heat transfer across the air regions, but as there is no discussion of it, and its residuals are omitted from their figures, it is assumed that radiation heat transfer was neglected. They provided temperature results for seven cases: an empty room, and 640 and 800 9975-cylindrical packages each generating 13, 16, and 19W.

Jacobs Engineering's simulations are highly relevant as they model heat generating boxes within a building. One uncertainty is their choice of HVAC diffuser. Their results show that the diffusers deflect all airflow toward the ceiling. This provides a more uniform distribution to all the boxes, as compared to the more typical diffuser design which blows air down on top of a few of the upper boxes. Most commonly, diffusers have fins that disperse the air passing through them, but do not fully reverse the direction of the airflow as it leaves the HVAC ducting. This may have been modeled in such a way to improve room temperature uniformity.

As there is no experimental data to validate the model discussed in this work, Jacobs Engineering's model will be duplicated as close as possible for reasonable verification. After verification, modifying the diffusers and rack system will be considered.

1.4. Large Room Computational Fluid Dynamics (CFD) Modeling

When thermal management is a concern in buildings, as is the case in radiological material staging buildings, thermal stratification will be a significant concern during the summer months as the heat from the roof will heat up the air close to the ceiling [5]. Another industry sensitive to thermal stratification is the cold storage food and fresh produce markets [5]. Porras-Amores, et al. collected experimental data and found that for five various wine storage warehouses throughout Spain, the differences in temperature throughout the room during the summer months proved to be a concern [5].

They found that a standard HVAC system with ceiling distribution vents for cold air will significantly reduce thermal stratification layers. The facilities with improved insulation such as the basement, earth-sheltered, and underground facilities were less affected by the hot summer months. They considered a basement warehouse that had two basement levels under two above ground levels of offices and industrial equipment. The earth-sheltered warehouse was first dug into the ground and then covered with 0.8m of irrigated vineyard gardens. The underground warehouse is similar to the earth-sheltered warehouse but utilizes the natural terrain as support instead of a concrete foundation.

The most relevant facility would be the above-ground air-conditioned warehouse, which is 38m long x 26m wide x 8m tall (125ft x 85ft x 26ft), roughly five times the size of the room modeled by Jacobs Engineering. It was found that the air closer to the ceiling is significantly warmer than that near the floor. This may be relevant to the current study because packages at the highest elevations of the staging facility may be in a higher temperature environment compared to ones nearer to the floor, and hence more prone to

overheating. However, Porras-Amores, et al. did not consider a facility that contained heat generating material [5].

Since buoyancy-driven warm air rises to the ceiling, thermal stratification has been found to be a significant issue for large warehouse heating during the winter [6]. The warm air gets trapped up high where the heat can escape through the roof. Wang, et al. performed both experiments and CFD simulations for two industrial warehouses, validating their model and testing different air mixing devices such as ceiling fans and bucket fans [6]. They modeled two rooms, one that is 12m long x 9.3m wide x 6.6m tall (39ft x 31ft x 22ft) and another that is 41.1m long x 17.5m wide x 6.9m tall (135ft x 57ft x 22ft). These are roughly half and three times the size of the room modeled by Jacobs Engineering. The k-ε turbulence model was used to accurately capture the turbulent flow leaving the fans. Additionally, the simulations had mesh sizes of 2.3 M elements, roughly one-fourth the size of the 10.3 M element detailed shelving Jacobs Engineering model. It was found that in cold climates the vertical temperature difference can reach 39°C (102°F) without a thermal destratification system, and with the system, the HVAC energy use could be reduced by 40%. Lastly, changing the HVAC duct diffusers can provide better mixing. The study showed that thermal stratification and accurate diffuser modeling will be important items to address in this work.

There are a variety of turbulence models available in commercially available CFD simulation packages. To determine scenarios under which particular models provide better performance, Zhang, et al. compared several models against each other and experimental data in four different scenarios [7]. The most relevant cases would be natural convection close to cold and hot walls, as well as forced convection in a room with partitions. The forced convection case is two dimensional and is 1m tall x 1.5m wide. The turbulence models compared include Renormalization Group (RNG) k-ε, SST k-ω, Large

Eddy Simulation (LES), and others. By comparing model accuracy and computing time, RNG k-ε proved most favorable. Results obtained with the SST k-ω model accurately predicted mean air temperature and had similar computing time but was less accurate with air velocity and turbulence. LES proved accurate all-around but had significantly longer computing times. For the purposes of modeling a nuclear staging facility, accurate temperatures are more important than airflow predictions. Since LES has long computing times and SST k-ω was found to be more conservative than RNG k-ε, SST k-ω was used as the computational resources available for the final predictive model is unknown.

Chapter 2: Computational Methods

In this chapter, the computational model for the staging room generated in the ANSYS package is described in detail. SolidWorks is used to generate a three-dimensional (3D) model of the staging building, including the lights, HVAC system, racks, and heat generating packages both as boxes and drums. ANSYS Workbench is then used to mesh the model, and CFD simulations are carried out using ANSYS Fluent. The geometry, mesh, and boundary conditions for the CFD simulations are described below.

2.1: Geometry

This work presents a model closely matching Jacobs Engineering's model, with slight modifications to the lighting, HVAC ducting, and racks to streamline the meshing process [3]. Figure 4 shows a 3D isometric view of the staging room model constructed in SolidWorks and is referred to as the rack-box model. It shows the lighting in red, HVAC supply in dark blue, HVAC diffuser in light blue, HVAC return in yellow, racks in green, and heat generating boxes in orange. Two additional models were created based on this design. Figure 5 shows that the floating-box model is identical to the rack-box model but excludes the racking system (the boxes are floating in the air). Figure 6 shows the third model, the floating-drum model which is similar to the floating-box model. The racks are excluded, and overall drum locations and room components such as the HVAC and lighting systems are the same. Figure 7 shows that the floating-drum model models four individual drums in the same location where one box was in the floating-box model. This creates 640 individual drums, which were previously approximated as 160 boxes that each represented four drums.

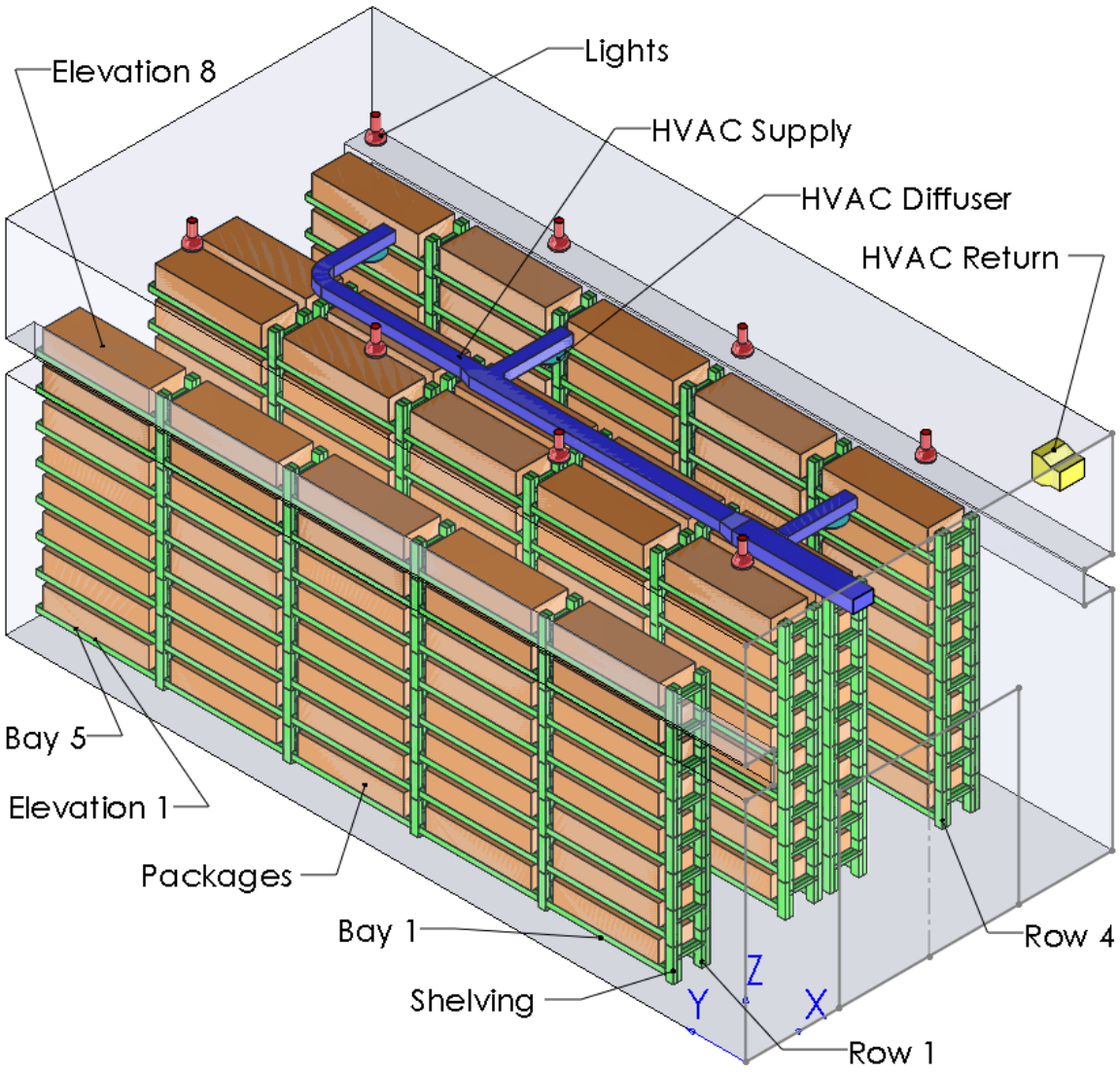

Figure 4: An isometric view of the rack-box model showing all the components modeled.

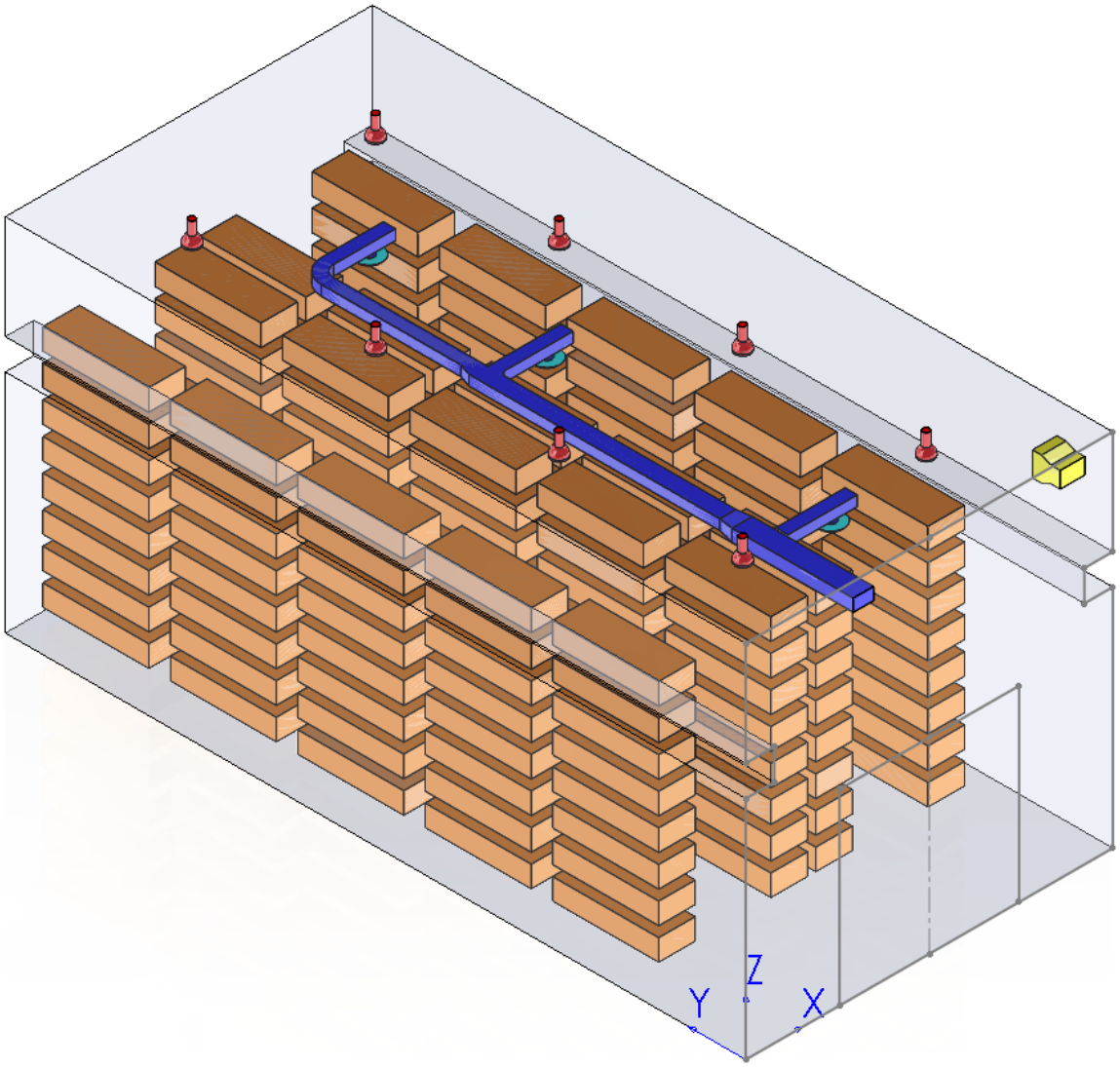

Figure 5: An isometric view of the floating-box model showing all the components modeled.

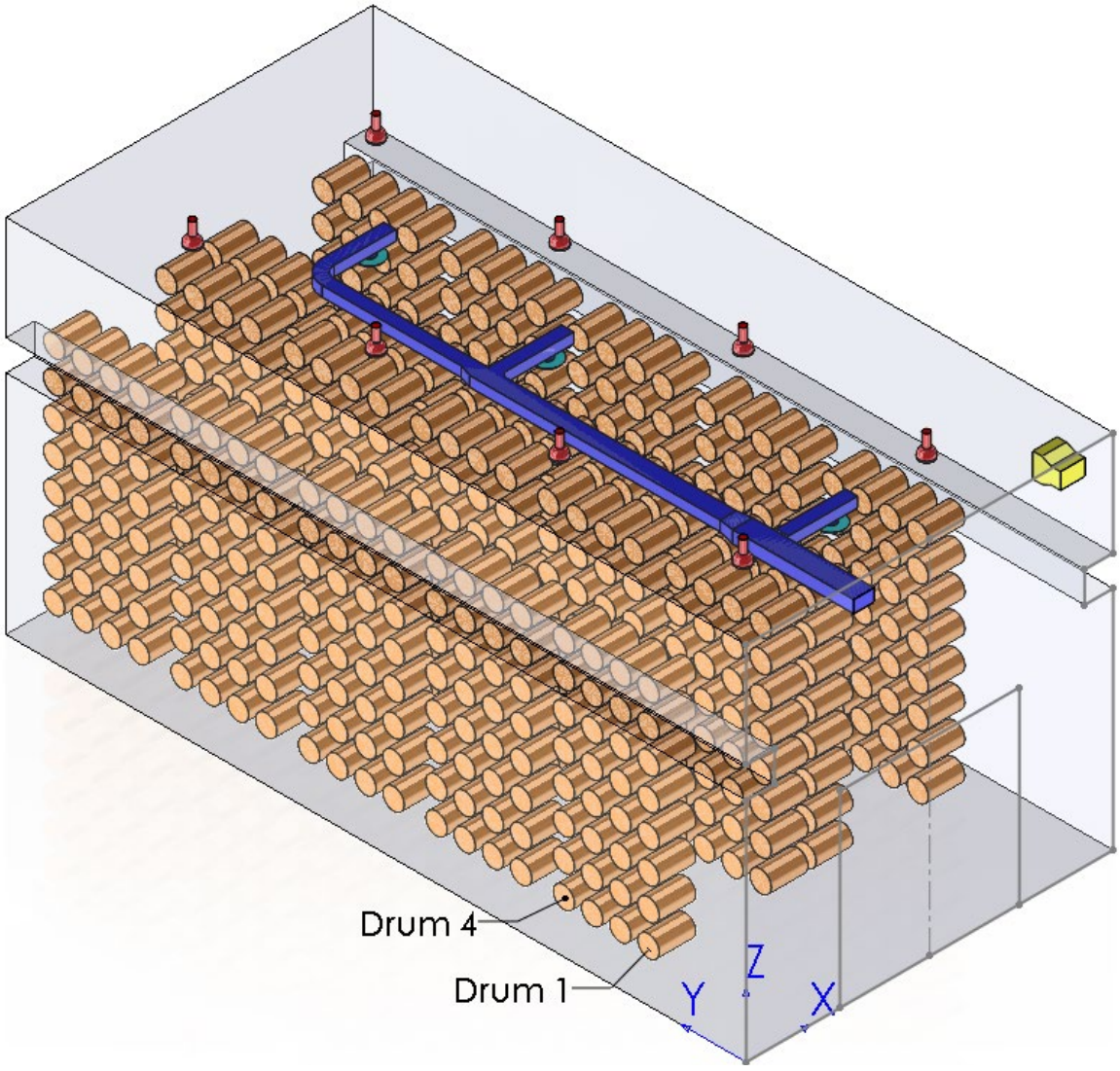

Figure 6: An isometric view of the floating-drum model showing the individual drums modeled.

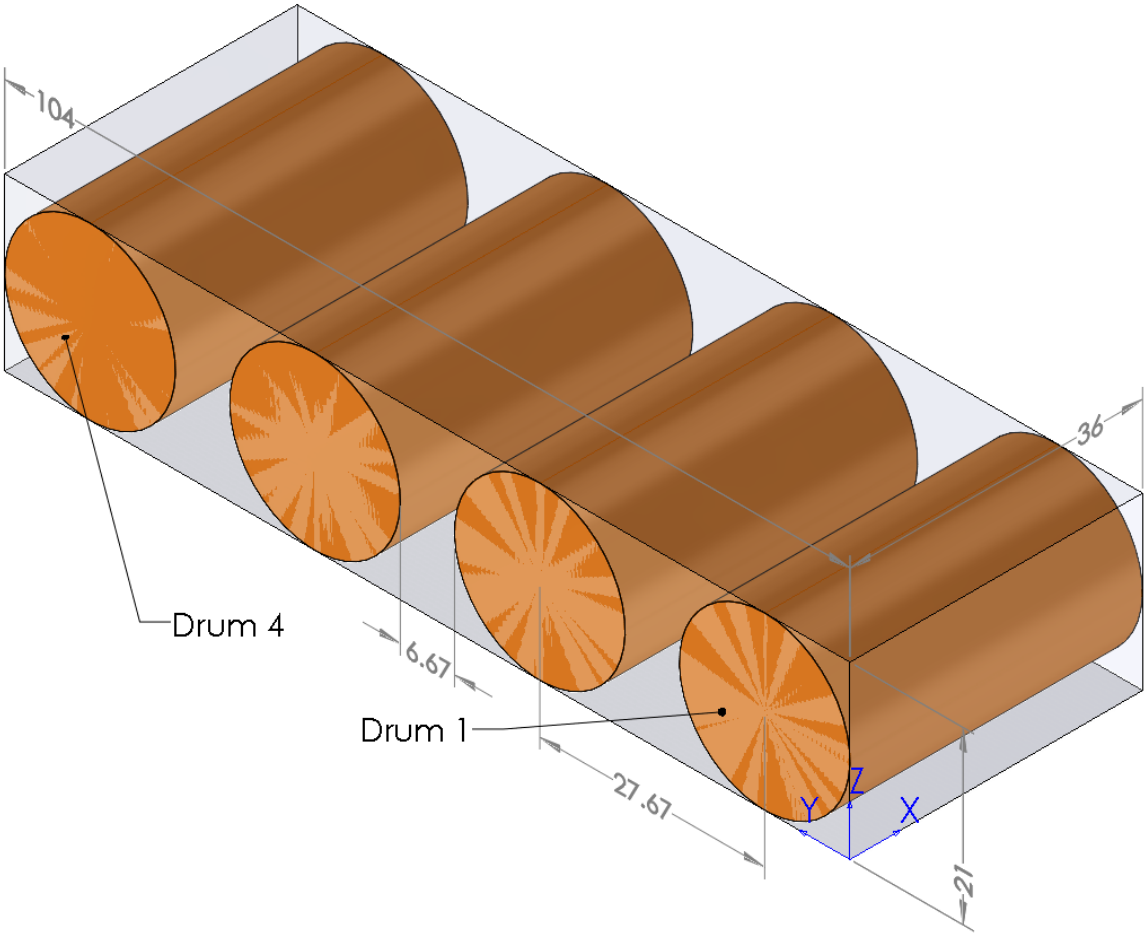

Figure 7: An isometric view of the drum model showing the drum naming inside of one bay. Dimensions are in inches.

Figure 8 shows the racking system which was approximated from Jacobs Engineering's figures due to a lack of dimensional information. The Jacobs Engineering racks had multiple cross members at 45° angles in the x-z planes on either end of a box. However, they were omitted in the current model for meshing simplification [3]. The rack material is 9.5 mm (0.375 in) thick SS 316. The main vertical (z-direction) and horizontal components (y-direction) are 20 cm (8 in) I-beams, the cross members supporting the boxes are 14 cm (5.625 in) square hollow tubing, and the short horizontal supports connecting the main vertical I-beams (x-direction) are 19 cm (7.625 in) wide by 8 cm (3.125 in) tall T-beams.

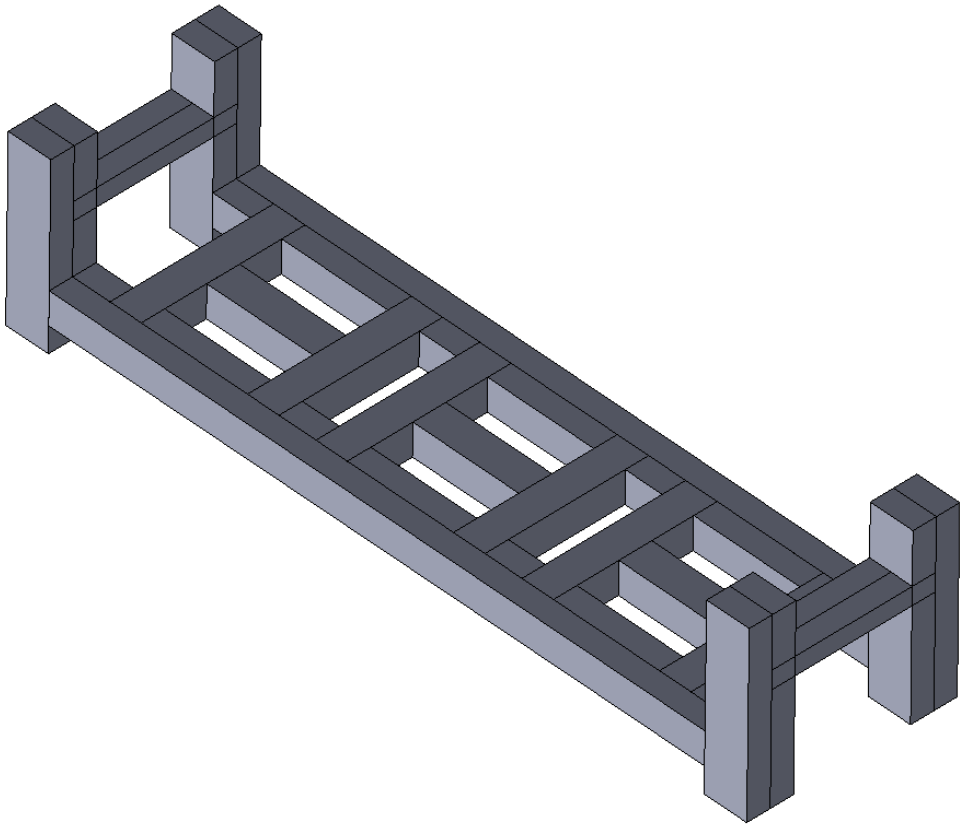

Figure 8: An isometric view of one rack bay showing the detail of the cross bracing.

The lighting mount was simplified to a constant-diameter rod instead of a multi-contour mount, and the light surface was simplified to a constant-radius curve instead of a multiple-radii surface. Figure 9 shows a close view of one of the lights. The lighting mount is modeled as aluminum, and the curved light bulb region is modeled as fluid enclosed by a thin wall.

Figure 9: A close-up view of one light showing the straight cylindrical mount and single-radius curved surface.

The HVAC ducting's diffusers were also approximated from Jacobs Engineering's figures [3]. Figure 10a shows a detailed view of a diffuser, with its walls shown in light blue. The diffuser was designed to redirect air coming from the HVAC ducts to the ceiling of the room. This design was chosen based on the streamlines from Jacobs Engineering flow plots. Figure 10b and Figure 10c show isometric views of the diffuser.

a.

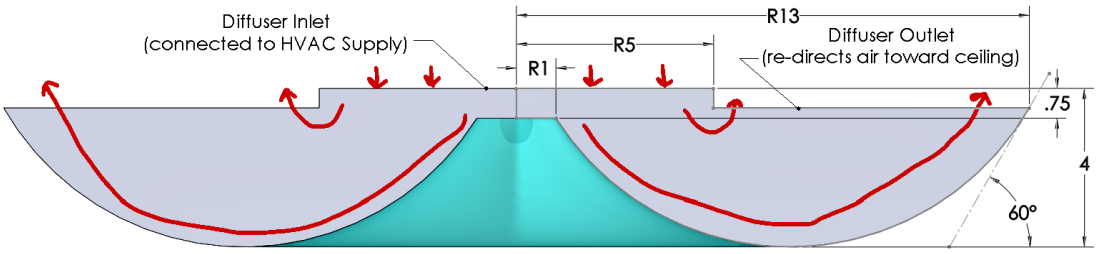

b.

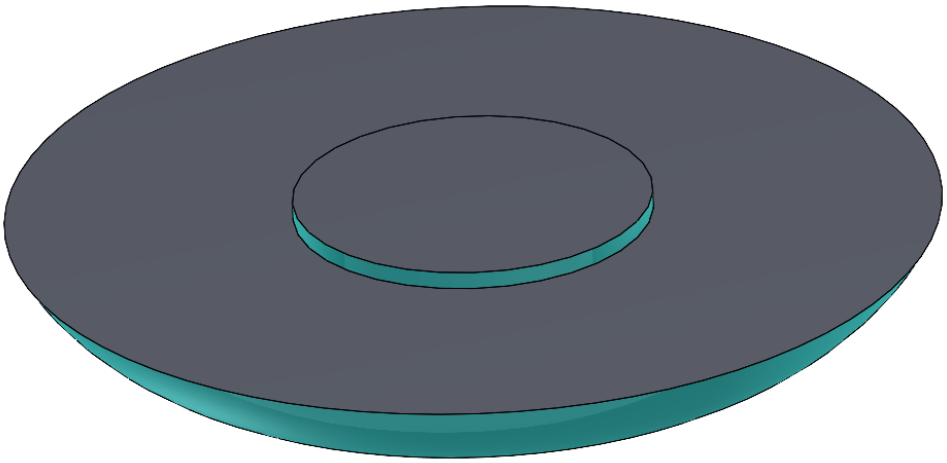

c.

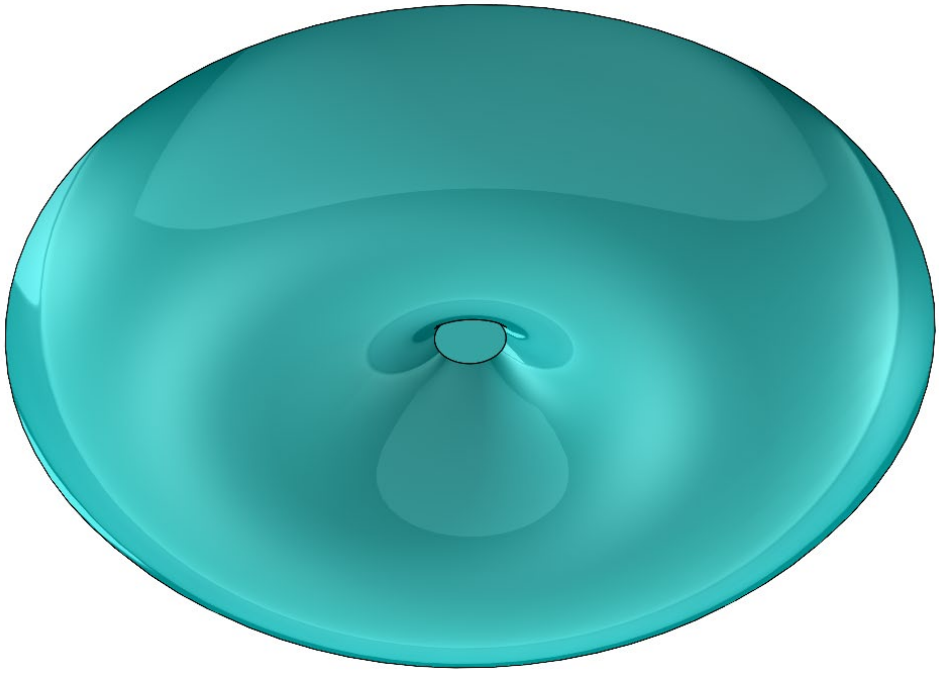

Figure 10: a) A cross-sectional view of the diffuser showing how airflow enters and leaves the diffuser with red arrows. Dimensions are in inches. b) An isometric view from above the diffuser showing the diffuser's mounting surface. c. An isometric view from below the diffuser showing the curved bottom wall of the diffuser.

To accurately identify individual boxes, it is beneficial to establish a naming convention and model origin. Figure 4 shows the model origin located at one corner of the door wall. The four rows are consecutively named in the positive x-direction, Row 1 through 4. Each row has five bays consecutively named in the positive y-direction, Bay 1 through 5. Each bay has eight elevations consecutively named in the positive z-direction, Elevation 1 through 8. Each box is identified by three numbers (Row, Bay, Elevation). For example, the box closest to the origin is identified as (1, 1, 1) and can be referred to as box 111. The box furthest from the origin is identified as (4, 5, 8) and can be referred to as box 458. Figure 7 shows that for the drum model, each bay contains four drums consecutively named in the positive y-direction, Drum 1 through 4. For the drum model, drums are named as (Row, Bay, Elevation, Drum). For example, the drum closest to the origin is identified as (1, 1, 1, 1) and can be referred to as drum 1111. The drum furthest from the origin is identified as (4, 5, 8, 4) and can be referred to as drum 4584.

2.2: Meshing

All three computational models generated for this study (rack-box, floating-box, and floating-drum models) were meshed in ANSYS Workbench. The “cutcell” cartesian method was used to generate the meshes. This method generates hex mesh elements in the bulk regions of the model. However, prism elements are created in the regions close to the model surfaces to accommodate the shape of the surfaces. A refined mesh can be obtained in the regions close to surfaces, and a coarse mesh can be obtained in the regions far from surfaces by combining eight elements into one element. This method was adopted because it uses a direct surface and volume approach without the need to decompose the model into small regions, which reduces the time and effort required for meshing. It also results in high-quality elements.

Figure 11, Figure 12, and Figure 13 show a cross-sectional view of the meshes generated for the rack-box, floating-box, and floating-drum models, respectively. These mesh views are the x-z plane that cuts through the centerline of the third diffuser, at y = 13.89 m (45 ft 6.75 in). These figures show that the mesh elements are refined close to the boxes, racks, diffusers, and lights (not shown in the figures). However, coarse elements are used in the bulk fluid regions of the staging room. It should be noted here that the floating-drum mesh view shown in Figure 13 does not cut through the centerline of the drums and as a result, they appear skinnier in diameter (shorter than the height of the boxes). The drum diameters are equal to the box heights. Figure 14 shows another cross-sectional view for the floating-drum model. This mesh view is the y-z plane that cuts through the centerline of the second row, at x = 4.01 m (13 ft 2 in). It shows the circular shape of the drums and the corresponding finer mesh around the drums due to the curved surfaces.

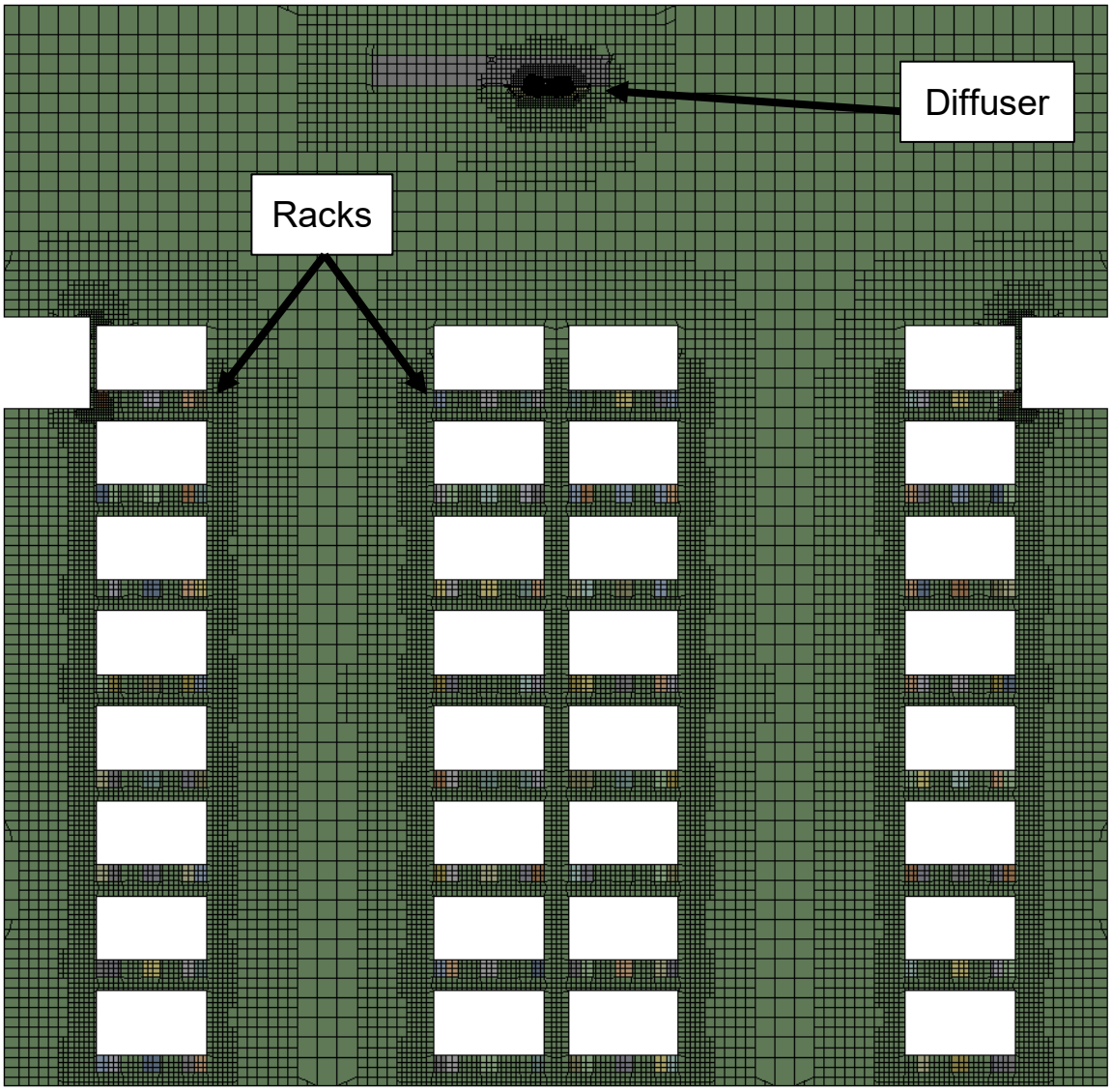

Figure 11: A cross sectional view of the rack mesh showing increased refinement around the racking system with a total of 9,111,995 elements.

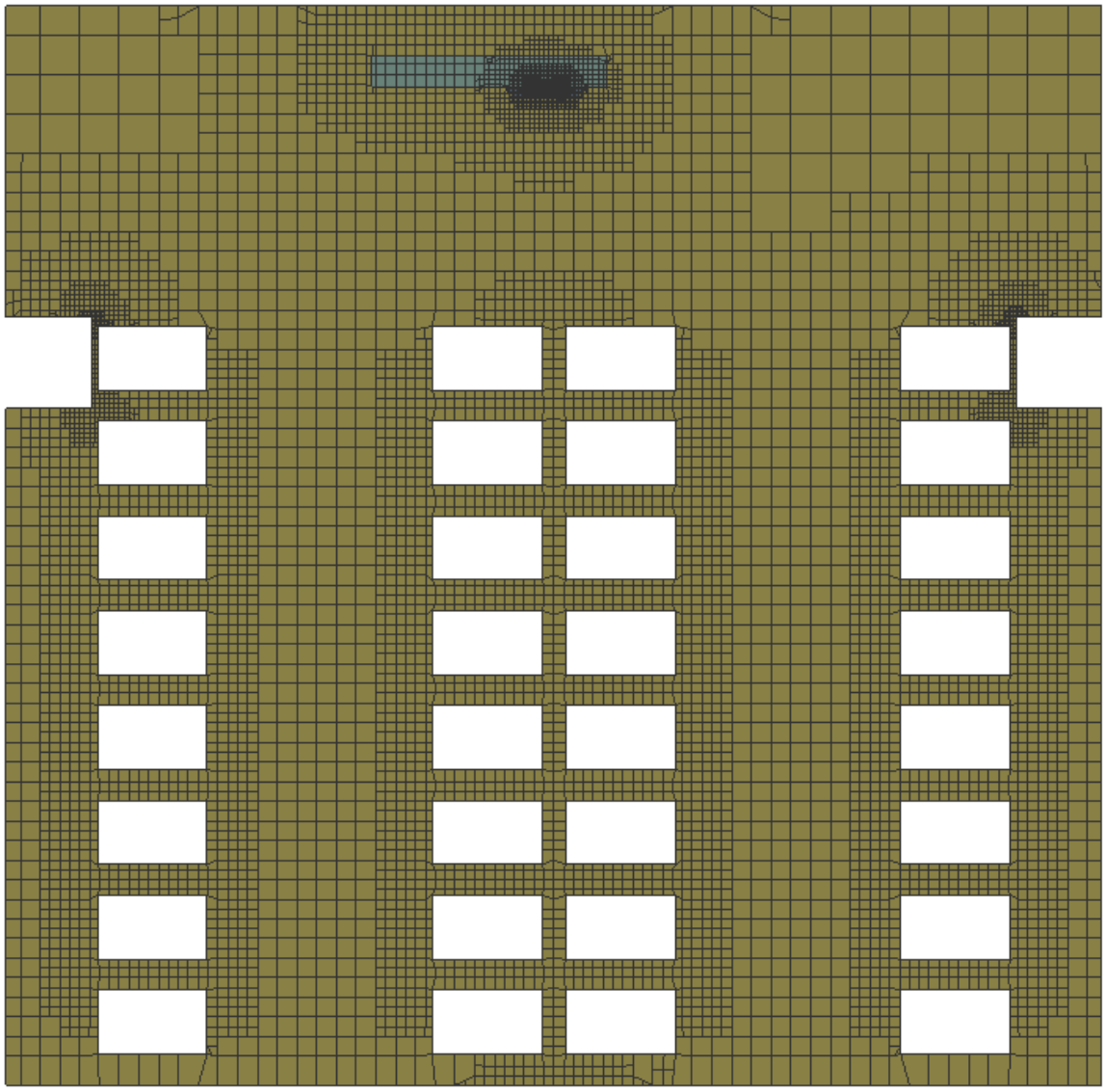

Figure 12: A cross sectional view of the nominal floating mesh showing increased refinement near the boxes and HVAC system with a total of 1,933,970 elements.

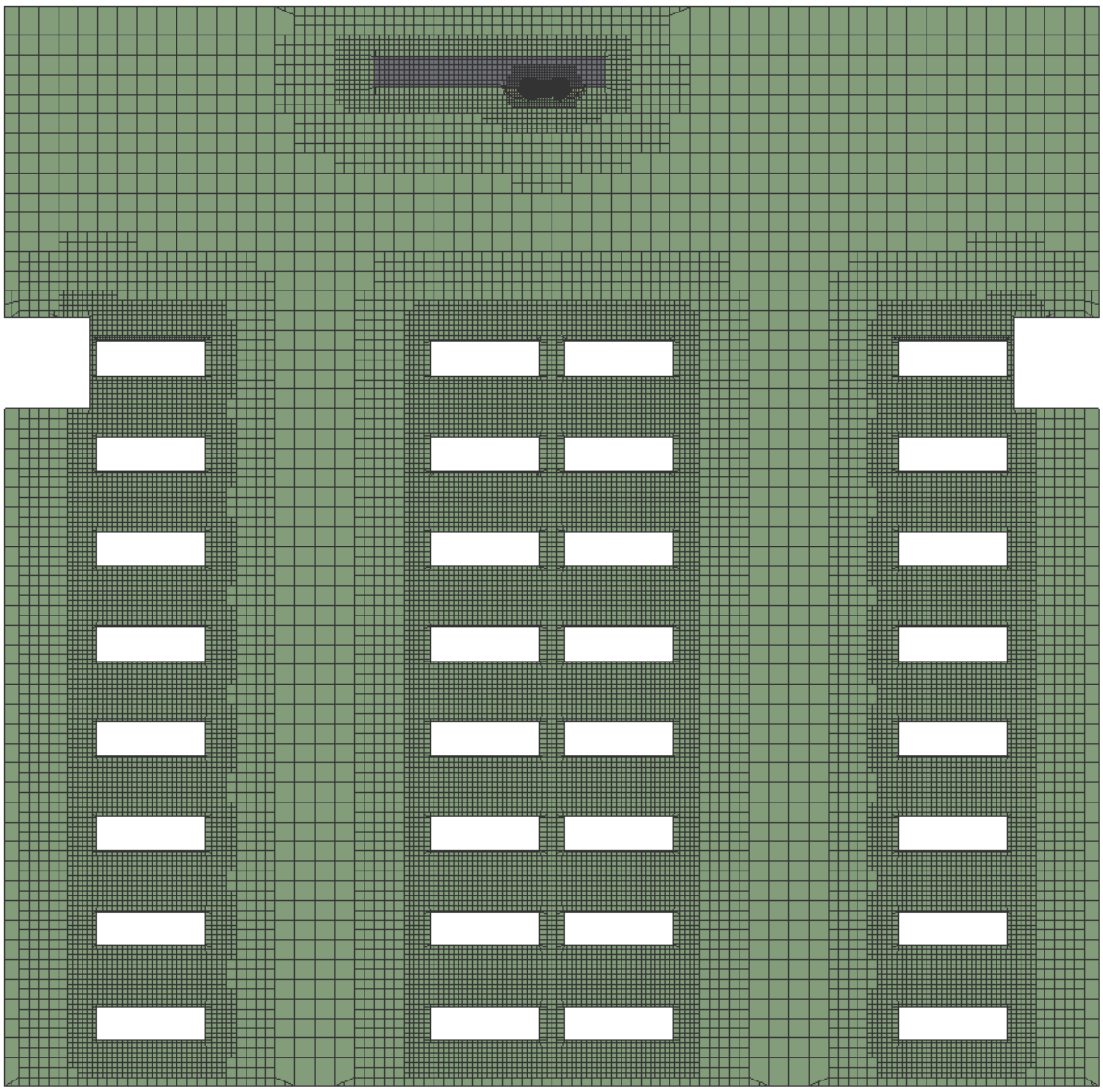

Figure 13: A cross sectional view of the accurate 640 floating-drum mesh showing individual drums modeled instead of boxes, with a total of 8,959,900 elements.

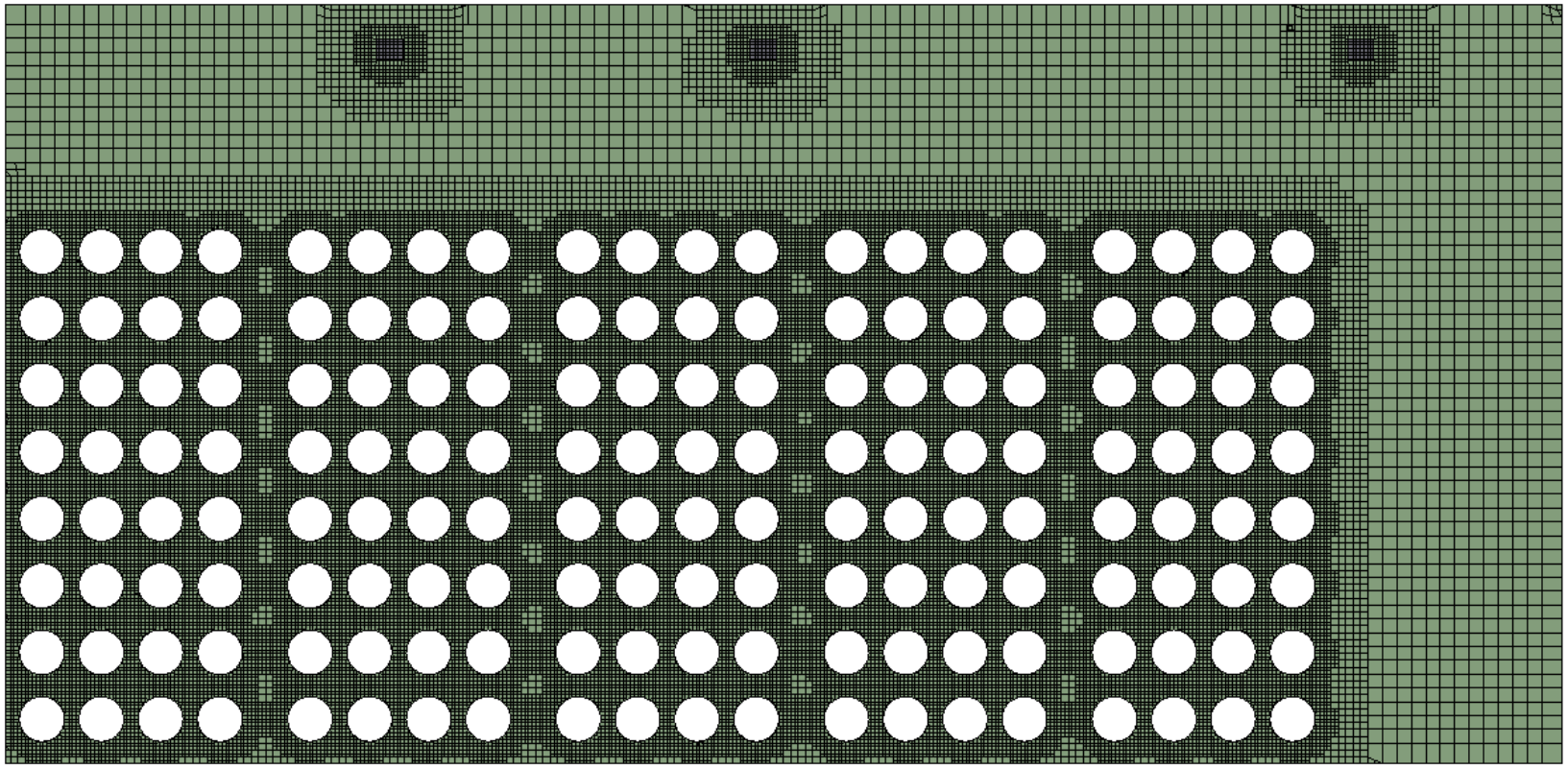

Figure 14: A cross sectional view of the accurate 640 floating-drum mesh showing increased refinement near the drums.

Figure 15 shows a cross-sectional view of the mesh generated for the floating-box 3.2 times mesh refinement study. This mesh view is the x-z plane that cuts through the centerline of the third diffuser, at y = 13.89 m (45 ft 6.75 in). The mesh is more refined than the nominal mesh throughout the entire model.

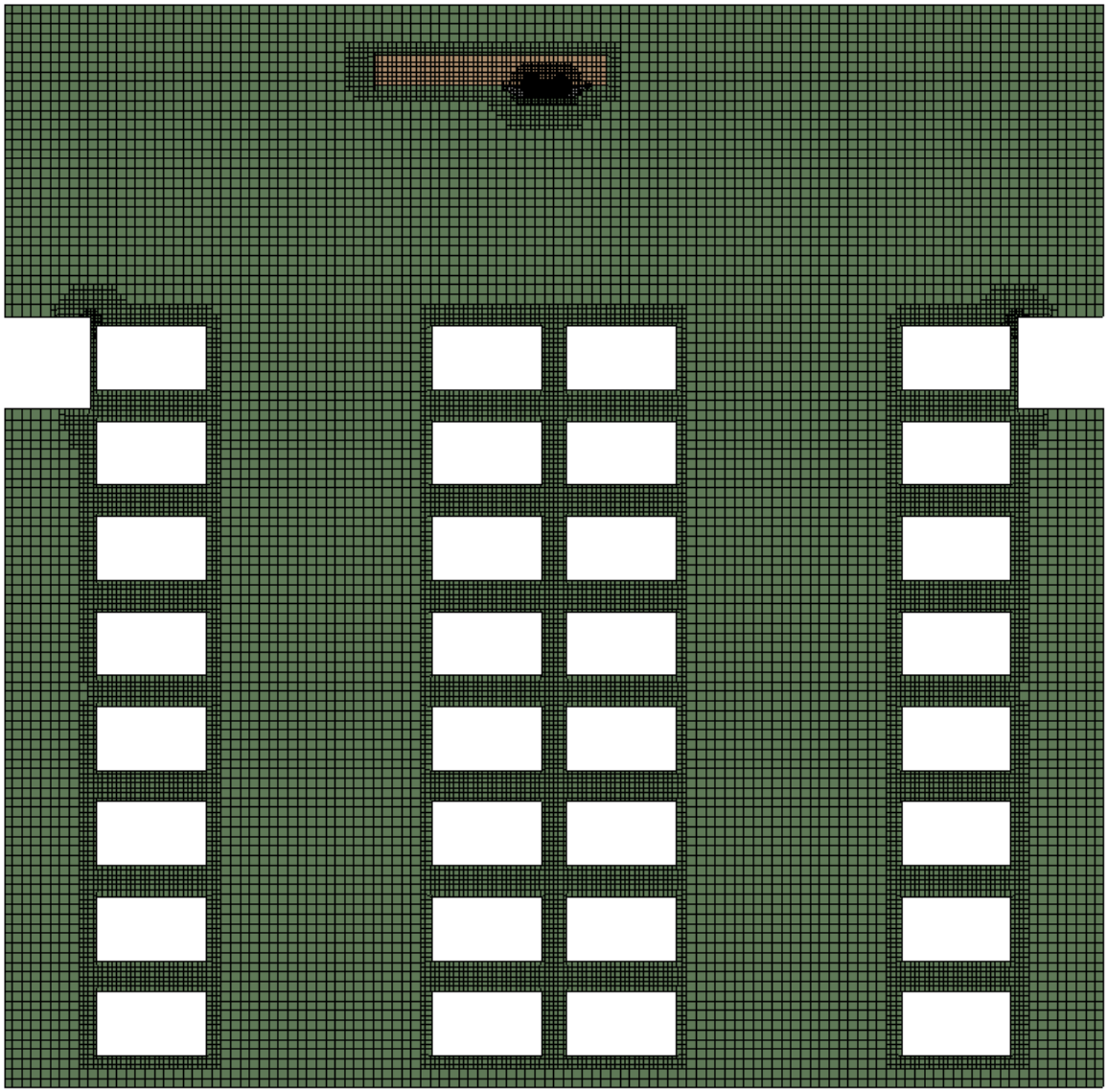

Figure 15: A cross sectional view of the 3.2 times refined mesh showing increased refinement throughout the room, with a total of 6,245,185 elements.

Table 2 summarizes Jacobs Engineering's model as well as the three models constructed for this work. A brief description of each model is also included. The rack-box model has the highest mesh element count due to the explicit modeling of the racks. This

model compares closely with Jacobs Engineering's model. The floating-drum model also has a large mesh element count due to the accurate modeling of each drum. The floating-box model resulted in the smallest number of mesh elements (more than 4 times smaller than the rack-box model). Therefore, a mesh sensitivity was conducted for the floating-box model. Table 3 gives the mesh element count for the nominal and 3.2 times refinement meshes. The results of the mesh sensitivity are presented in the Results Chapter.

Table 2: The mesh size for the models generated in this work, compared to Jacobs Engineering's model.

Mesh Name	Mesh Size (Elements)	Mesh Description
Jacobs Engineering [3]	1.03E+07	160 boxes with racks
Rack-box	9.11E+06	160 boxes with racks
Floating-box	1.93E+06	160 boxes, floating, without racks
Floating-drum	8.96E+06	640 individual floating cylindrical drums are modeled

Table 3: A mesh refinement study conducted on the nominal floating-box mesh.

Mesh Name	Mesh Size (Elements)
Nominal	1.93E+06
3.2 times Refinement	6.25E+06

2.3: Numerical Simulations and Boundary Conditions

Steady-state CFD simulations are performed in ANSYS Fluent for different package heat generations. The external walls, floor, and ceiling are modeled as adiabatic, assuming no heat transfer to the building's exterior. This is a conservative assumption as some heat will be exchanged to the building's exterior. The HVAC system supplies air at atmospheric pressure with a mass flow rate of 0.784 kg/s, density of 1.213 kg/m^3, and temperature of 18°C (1370 ACFM, 64°F), and allows air to freely exit the room via one zero pascal gauge pressure return outlet. Each light generates 100W of heat, which is

applied only in the curved light bulb volume region, and not within the lighting mount. Therefore, the eight lights generate a total of 800W.

The box and drum internal volumes were not modeled. Therefore, a surface heat flux equal to the heat generation of one box or drum divided by the surface area of one box or drum is applied on all surfaces of each box or drum. This is not completely valid, as certain locations of the drum will have a higher surface heat flux than others. While this may have some effects on the temperature distribution across that package's surface, the average temperature of the package and the global temperatures of the model should not be significantly affected. However, a study could be conducted to verify this assumption. Three package heat generations are considered in this study (13, 16, and 19W per drum). The 19W per package represents the maximum allowable heat generation of a 9975 drum [2]. It should be reminded here that each box represents four single packages (or drums). Therefore, the total heat generation of the boxes is four times that of a single package. The room total heat generations for all the packages including the lights are 9,120W, 11,040W, and 12,960W.

Conductive heat transfer within the solid and air regions and radiation heat transfer across the air regions are modeled. Natural and forced convection in the air regions is also modeled. An emissivity value of 1 is used for all the surfaces since actual surface properties are unknown, and the goal of the model is to be applicable for a wide range of radiological packages and racking systems. All fluid regions are modeled as air under incompressible, ideal gas assumptions with a pressure-coupled model.

Chapter 3: Results

This work is performed in two stages.

3.1: Box-package Model

In the first stage, we perform ANSYS/Fluent simulations that are intended to reproduce the results calculated by Jacobs Engineering [3]. Jacobs Engineering used Star-CCM+ simulations that employed box-packages to represent sets of four drum-packages within each shelving bay. In this stage, we perform scoping simulations for two purposes. The first is to quantify the effects of including or excluding certain physical and modeling phenomena on both the average predicted package temperatures, and the computational resources and time required to perform each simulation. These phenomena include radiation heat transfer, unsteadiness, and inclusion of the racks. The second purpose is to determine how closely our results compare with Jacobs Engineering's results. This quantifies the dependence of the results on the CFD code employed, small variations in the geometry, and the method used to create the computational mesh.

Predictive simulations employing a highly refined mesh that includes all components of the packages and rack system, models the effects of thermal radiation, and explicitly models flow unsteadiness can be performed. However, those simulations would be highly computational resource and time intensive. The goal of this stage is to determine the level of simplification that can be employed in a predictive model while maintaining results similar to a highly detailed model.

3.1.1: Most Complete Model

For the current work, we first present results from our most complete model, and then compare it to simulations that are less complete. The most detailed model is a transient simulation of the rack-box-package model, including radiation heat transfer. The model was found to achieve a quasi-steady state and is transient due to turbulence in the room. This caused difficulty in convergence with a steady state simulation, requiring the transient simulation to be conducted to decrease the simulation's residuals. Although we are interested in the steady state results of the system, the transient results achieve better residuals. The initial conditions for the transient simulation are the quasi-steady state values obtained from a steady state simulation. To determine the timestep used, the Courant Friedrichs Lewy stability criteria (CFL Number) was employed. The global timestep of the system is defined as

$$\Delta t_{global} = \frac{CFL_{global}}{\max(\sum \frac{outgoing\ fluxes}{volume})} . \quad (1)$$

The ratio $\sum \frac{outgoing\ fluxes}{volume}$ is calculated for each element [8]. CFL_{global} was set equal to 2 in most cases, and a value of 20 did not appear to vary the results.

All transient simulations compute 1 second of simulation time, during which the results were found to be quasi-steady for the second half of the simulation. Therefore, temperature values reported are averaged from 0.5-1s.

Figure 16 shows a full isometric view of the temperature contours of the box-package surfaces. The surface temperatures are nearly uniform. However, box-packages close to the ceiling and door wall are somewhat cooler due to their proximity to the HVAC air diffusers and return ducting.

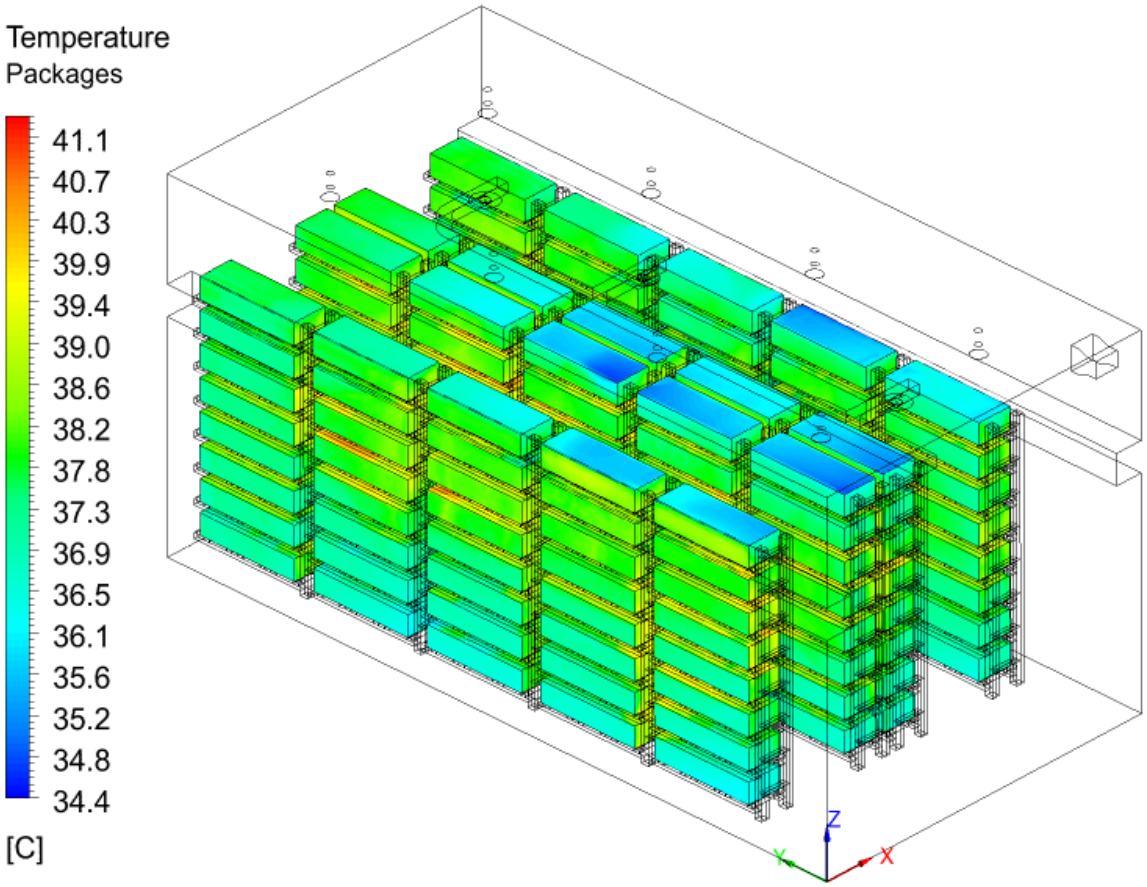

Figure 16: Rack-box-package full isometric view.

Figure 16 also shows that the upper surfaces of some of the box-packages near the mid-height are warmer than most surfaces. Figure 17 shows the same temperature contour data as Figure 16, but with the first two rows removed to show the warmer regions. It shows that the side and top box-package surfaces near the mid-height of the racks exhibit the highest temperatures.

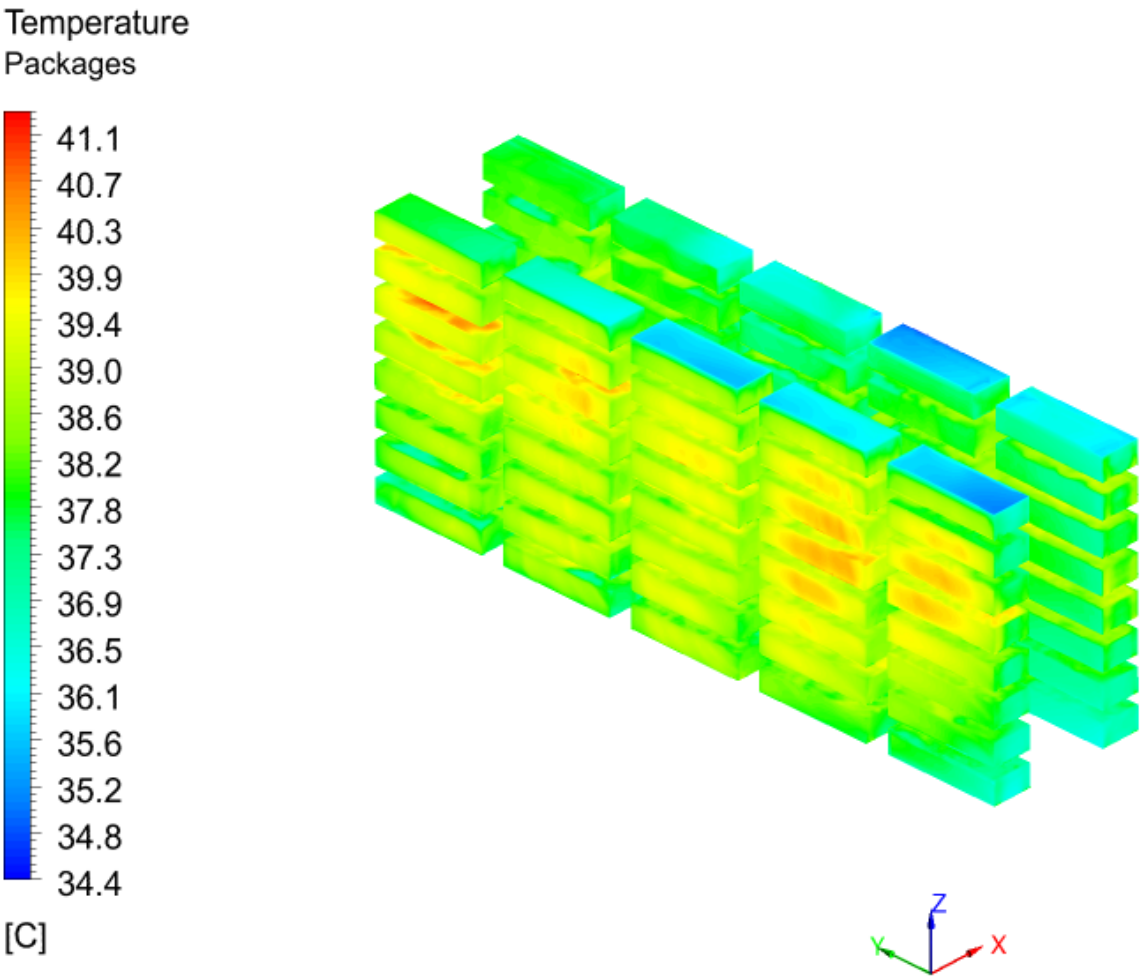

Figure 17: Rack-box-package half isometric view.

Figure 18 shows the airflow pattern and temperature contours in a plane in the middle of the first aisle, at x = 2.6m (8ft 7in). The velocity vectors shown are the tangential components of the air velocity in that plane, with the length of the vectors representing a range from 0-0.6m/s. Results from the other aisle are similar and therefore are not shown. There is one large recirculating flow eddy, with air flowing toward the door wall at higher elevations, and away from the door wall close to the floor. There is a significant downdraft of cool air along the door wall.

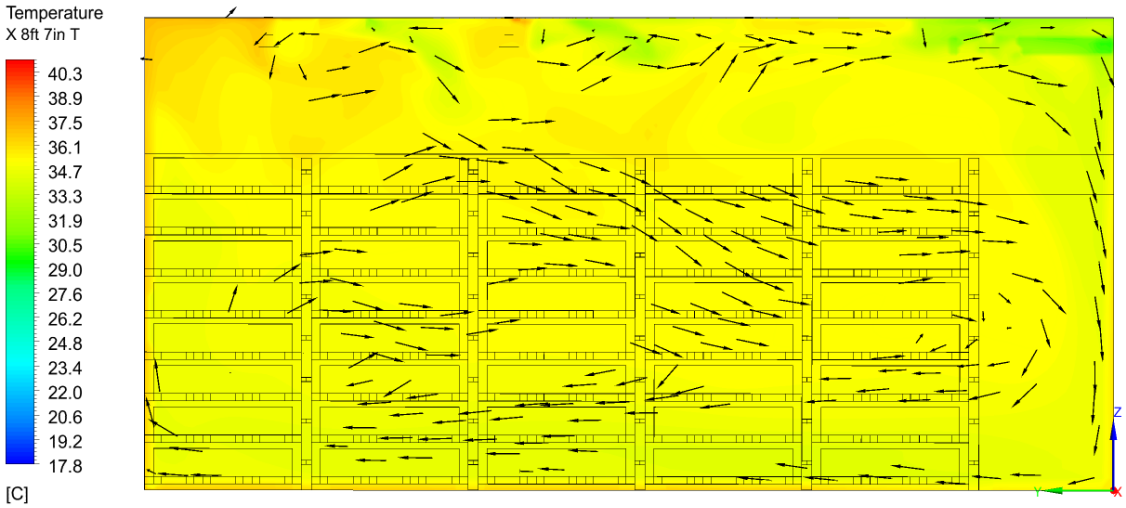

Figure 18: Rack-box-package first aisle, x = 2.6m (8ft 7in).

As all the box-packages generate heat, warming the surrounding air, the air far from the door rises. This air then pushes the air that is close to the ceiling toward the door, where it is also cooler. The cool air sinks along the door wall and flows into the box-package area, repeating the process.

Figure 19 shows the airflow pattern and temperature in the narrow gap between the two racks in the middle of the room, at x = 4.6m (15ft 0in). The velocity vectors shown are the tangential components of the air velocity in that plane, with the length of the vectors representing a range from 0-2.1m/s. Air near the upper box-packages is slightly warmer than the air at the same height in the first aisle shown in Figure 18. The narrow gap between the second and third rows has purely upward flow, with downward flow in the large air region between the box-packages and the door. The warm air from the box-packages strictly rises toward the ceiling, without much horizontal or downward flow. The cool air exiting the diffusers is pushed toward the door wall, where it sinks. The air then flows into the box-package area.

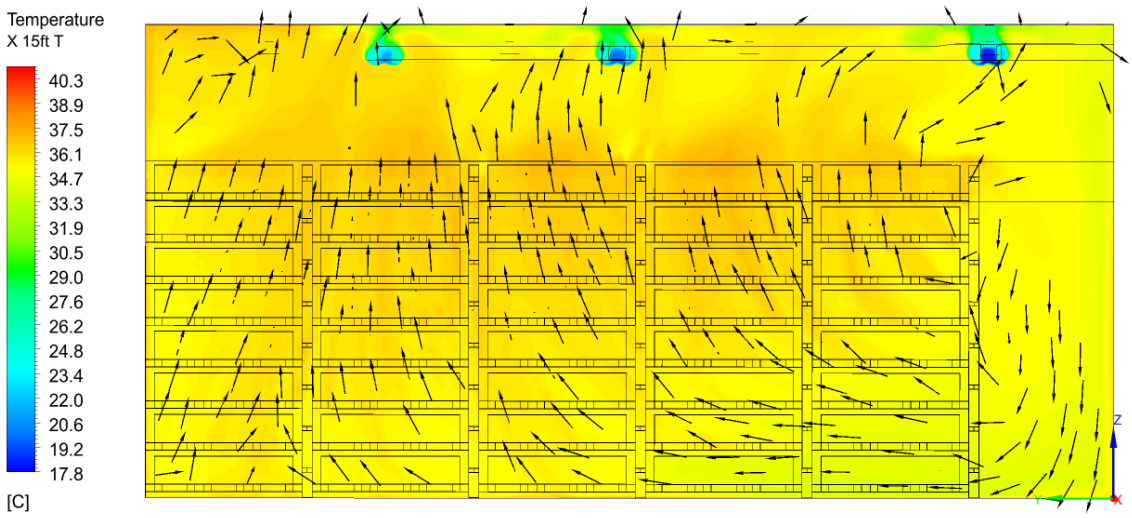

Figure 19: Rack-box-package room center, x = 4.6m (15ft 0in).

Figure 20 shows the airflow pattern and temperature in the middle of the third row, at x = 5.1m (16ft 10in). This row was selected because it contains the hottest box-package. The velocity vectors shown are the tangential components of the air velocity in that plane, with the length of the vectors representing a range from 0-1.1m/s. In this plane, some air is blocked vertically between different elevations of box-packages which inhibit its flow and creates localized hot spots both above and below individual box-packages for multiple bays and elevations. Additionally, plumes of warm air rise in between the rack bays as these are the main regions within the rows where warm air is not obstructed by the box-packages from rising.

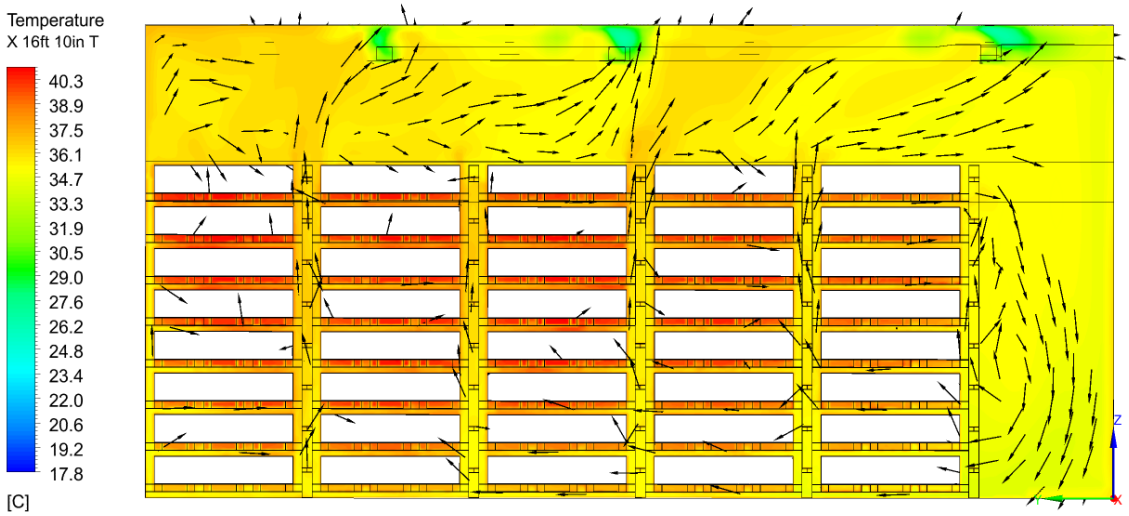

Figure 20: Rack-box-package third row, x = 5.1m (16ft 10in).

Figure 21 shows the airflow pattern and temperature at the mid-height of the room, at z = 4.5m (14ft 9in). The velocity vectors shown are the tangential components of the air velocity, with the length of the vectors representing a range from 0-0.6m/s. This figure supports the conclusion that air at higher elevations flows toward the door, and that there is sinking cold air near the door. Unfortunately, this means that when the room door is opened, much of the cool air from the HVAC system may escape. An air curtain could be placed at the doorway to help reduce this temporary reduction in cooling capacity.

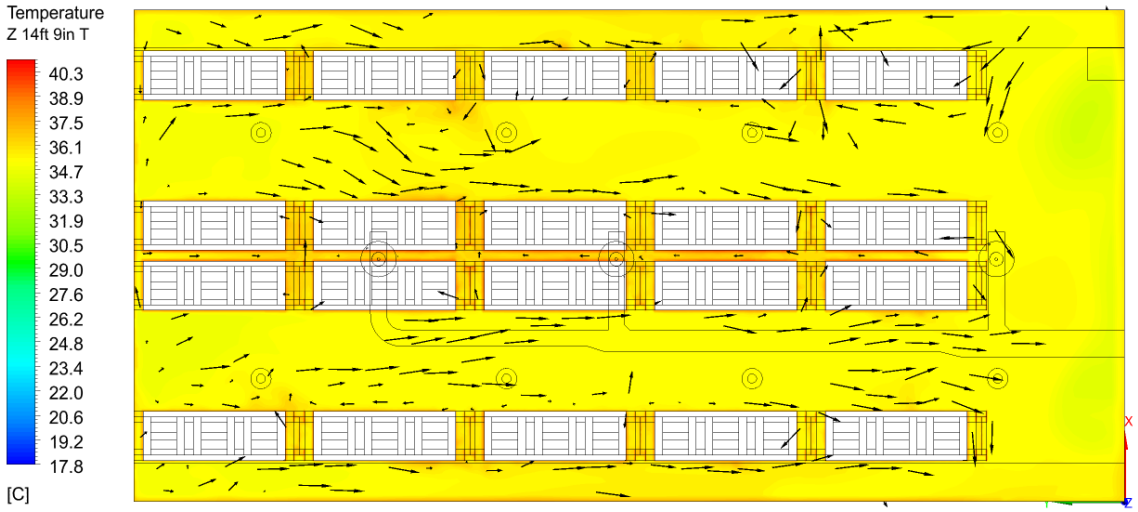

Figure 21: Rack-box-package room center, z = 4.5m (14ft 9in).

3.1.2: Box-package Model Variations Summary

For the box-package models, several scoping simulations were performed to determine the effects of various model conditions on both the surface temperature of the box-packages and simulation resource cost. Table 4 summarizes the Condition Number and Condition Name for each condition. For Condition Numbers 2 through 9, the Condition Name describes the difference between that condition and Condition 1.

Table 4: Summary of all 17 box-package simulations performed in this work. Jacobs Engineering results are also included [3].

Condition Number	Condition Name	Time Dependence	Radiation Heat Transfer	Racks	Mesh	Turbulence Model	Q_D [W]
Current Work							
1	Most Complete	Transient	Included	Yes	9.1E+06	SST k-ω	19
2	Steady	Steady		Yes	9.1E+06	SST k-ω	13, 16, 19
3	Steady Floating	Steady		No	1.9E+06	SST k-ω	13, 16, 19
4	Steady Floating RNG	Steady		No	1.9E+06	RNG k-ε	19
5	No Rad	Transient	Excluded	Yes	9.1E+06	SST k-ω	19
6	No Rad Steady	Steady		Yes	9.1E+06	SST k-ω	13, 16, 19
7	No Rad Steady Floating	Steady		No	1.9E+06	SST k-ω	13, 16, 19
8	No Rad Steady Floating Refined	Steady		No	6.2E+06	SST k-ω	13, 19
Earlier Work							
JE [3]	Jacobs Engineering	Steady	Unknown	Yes	1.0E+07	SST k-ω	13, 16, 19

Table 4 includes the current work's 8 conditions performed, as well as Jacobs Engineering's (JE) earlier work [3]. Table 4 specifies each condition's time dependence, inclusion of radiation heat transfer, inclusion of racks, mesh size, turbulence model used, and drum-package heat generation rate. Conditions were either conducted as transient or steady state simulations. Table 4 shows which conditions included radiation heat transfer, and those which excluded it. Additionally, certain conditions included the racks while others did not. The mesh size for each condition is given, as well as the turbulence model employed. The heat generation of the drum-packages is given as Q_D, in Watts per drum-package. Since each box-package represents four drum-packages, the total heat dissipated by each box-package is 4 x Q_D.

For each condition, simulations for one, two, or three heat generations are conducted. This brings the total number of box-package simulations to 17. When referring to a specific simulation, the notation of Simulation <number>-<drum-package heat generation rate> will be used. For example, the simulation for Condition 1 with a drum-package heat generation rate of 19W is Simulation 1-19W. The conditions that included radiation heat transfer, Conditions 1 through 4, utilized an emissivity of $\epsilon = 1$ on all surfaces throughout the room.

Table 5 summarizes select results from all 17 simulations conducted in the current work, as well as Jacobs Engineering's earlier work [3]. For each simulation, the drum-package heat generation rates used are listed. The rack, bay, and elevation location of the hottest box-package is also provided. In this table, $\Delta T_{B,Max}$ is the average surface temperature of the hottest box-package in the room minus the inlet temperature, T_I = 17.8°C (64°F) for all simulations. The hottest package is important in a predictive model because it is likely to be the one whose component temperatures have the smallest safety

margins when compared to the respective component temperature limit. $\Delta T_{B,Avg}$ is the average surface temperature of all box-packages in the room minus T_I.

Table 5: The location and temperature of the hottest box-package for both current work and Jacobs Engineering. The average box-package temperature and resource cost is also included for the current work.

Condition Number	Q_D [W]	Location of hottest box-package			$\Delta T_{B,Max}$ [C]	$\Delta T_{B,Avg}$ [C]	RC [Core-hr]	Operating System
		Rack	Bay	Elevation				
1	19	2	4	6	21.9	20.5	37,700	Linux (120 Cores)
2	19	2	3	6	22.0	20.6	4,800	Linux (120 Cores)
	16	2	3	6	19.2	17.9		
	13	2	3	6	16.0	14.9		
3	19	3	3	5	22.0	20.4	1,300	Linux (120 Cores)
	16	3	3	5	18.9	17.5		
	13	3	3	5	16.1	14.8		
4	19	3	3	5	21.8	20.2	1,000	Windows (32 Cores plus 1 GPU)
5	19	2	5	7	23.7	22.4	6,500	Linux (120 Cores)
6	19	2	5	8	23.5	22.4	1,100	Linux (120 Cores)
	16	2	5	8	20.2	19.3		
	13	1	4	6	17.2	16.2		
7	19	3	5	7	23.7	21.8	300	Windows (32 Cores plus 1 GPU)
	16	3	5	7	20.5	18.9		
	13	3	5	7	17.2	15.7		
8	19	3	5	7	23.0	21.4	800	Windows (32 Cores plus 1 GPU)
	13	3	5	7	16.4	15.3		
Jacobs Engineering [3]	19	2	3	6	23.7	22.2	Unknown	Unknown
	16	2	2	6	20.6	19.2		
	13	2	3	8	17.3	16.2		

Table 5 also summarizes each condition's resource cost, RC, which is equal to the number of computational cores employed to run a simulation times the amount of time required to complete a simulation in hours. RC is roughly the same for all simulations within the same condition, as the only change within the same condition is the drum-package heat generation rate, which does not significantly affect RC. The operating

system used for each condition is also included as ANSYS/Fluent's computational efficiency may depend on the operating system.

Table 5 shows that the location of the hottest box-package varies for each simulation. For the current work, the rectangular prism region between Rack 1, Bay 3, Elevation 5 and Rack 3, Bay 5, Elevation 8 contains the hottest box-package regardless of the simulation. For all simulations, the hottest box-package is at most 1.8°C (3.3°F) warmer than the average box-package surface temperature, occurring for Simulation 7-19W.

Table 5 shows that, for conditions in which different Q_D values are considered, the temperature differences increase with Q_D. While the temperature differences for a given value of Q_D are similar for different conditions, they are not the same. Finally, the resource cost for different conditions varies significantly. For example, the resource cost for the transient simulation Condition 1, is roughly 7.8 times that for the steady state simulations in Condition 2. The rack-box-package Conditions 2 and 6 are 3.7 times more computationally expensive compared to the floating-box-package Conditions 3 and 7. Additionally, including radiation heat transfer in Condition 1 is 4.5 times more computationally expensive compared to Condition 5 with no radiation heat transfer.

3.1.3: Global Results

Figure 22 and Figure 23 show $\Delta T_{B,Avg}$ versus Q_D for all conditions listed in Table 4. Conditions that include racks are shown with solid symbols, and those excluding racks are shown with open symbols.

Figure 22 shows results from Conditions 1 through 4, which include radiation heat transfer. Results reported by Jacobs Engineering are also included [3]. Simulation 1-19W includes time-dependent effects, racks, and radiation heat transfer for Q_D = 19W. Only one

heat generation rate was simulated for Condition 1 because it requires significant computational resources and time. Steady state results that include radiation heat transfer are presented for both rack-box-package and floating-box-package Conditions 2 and 3 for three heat generation rates. Additionally, one steady state floating simulation was performed using the RNG k-ε turbulence model (Simulation 4-19W).

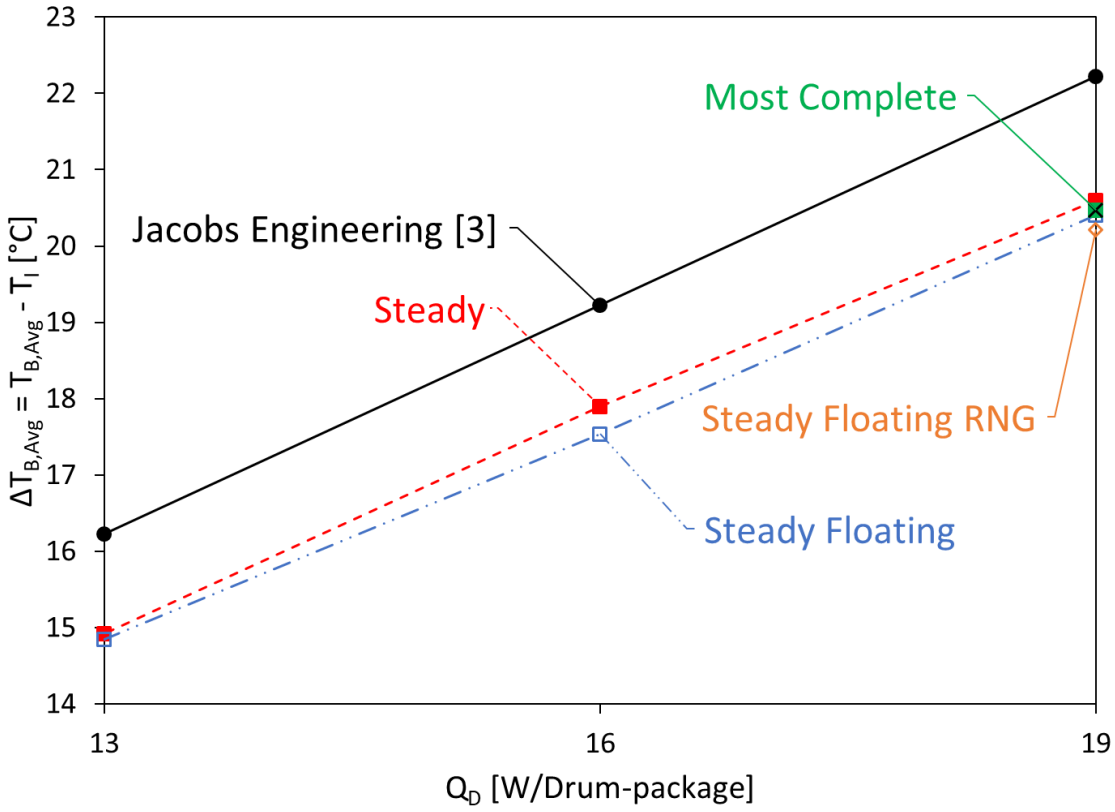

Figure 22: Difference between the average package surface temperature and room inlet temperature versus drum-package heat generation rate. All the current simulation results in this plot include radiation heat transfer. Results are shown with and without racks, for both steady state and transient Conditions. Results from Jacobs Engineering are also included [3].

Figure 22 shows that results from the Most Complete and Steady simulations give very similar results (Simulation 1-19W and 2-19W). Simulation 1-19W, Most Complete, is only 0.1°C (0.2°F) cooler than Simulation 2-19W, Steady. However, the transient simulations require significantly more computational resources. Condition 3, Steady

Floating, gives temperatures that are at most 0.6°C (1°F) cooler than Condition 2, Steady, and requires significantly less computational resources. Simulation 4-19W, which employed the RNG k-ε turbulence model, is used for a turbulence model comparison [8]. All other conditions in the current work used the SST k-ω turbulence model [7]. The average box-package surface temperature predicted by the RNG k-ε model is 0.2°C (0.3°F) cooler than Simulation 3-19W that used the SST k-ω turbulence model. This comparison is not exhaustive. However, the small difference between model results suggests the choice of turbulence models does not significantly affect the relevant computational results. Since Jacobs Engineering also used the SST k-ω turbulence model, we use it in the remaining simulations. However, before developing a predictive model, an extensive turbulence model study should be conducted.

The Jacobs Engineering and current results show that increasing Q_D from 13 to 19W increases the average box-package surface temperature by approximately 6.1°C (11°F). However, current results give temperatures that are approximately 1.7°C (3°F) cooler than the Jacobs Engineering calculations.

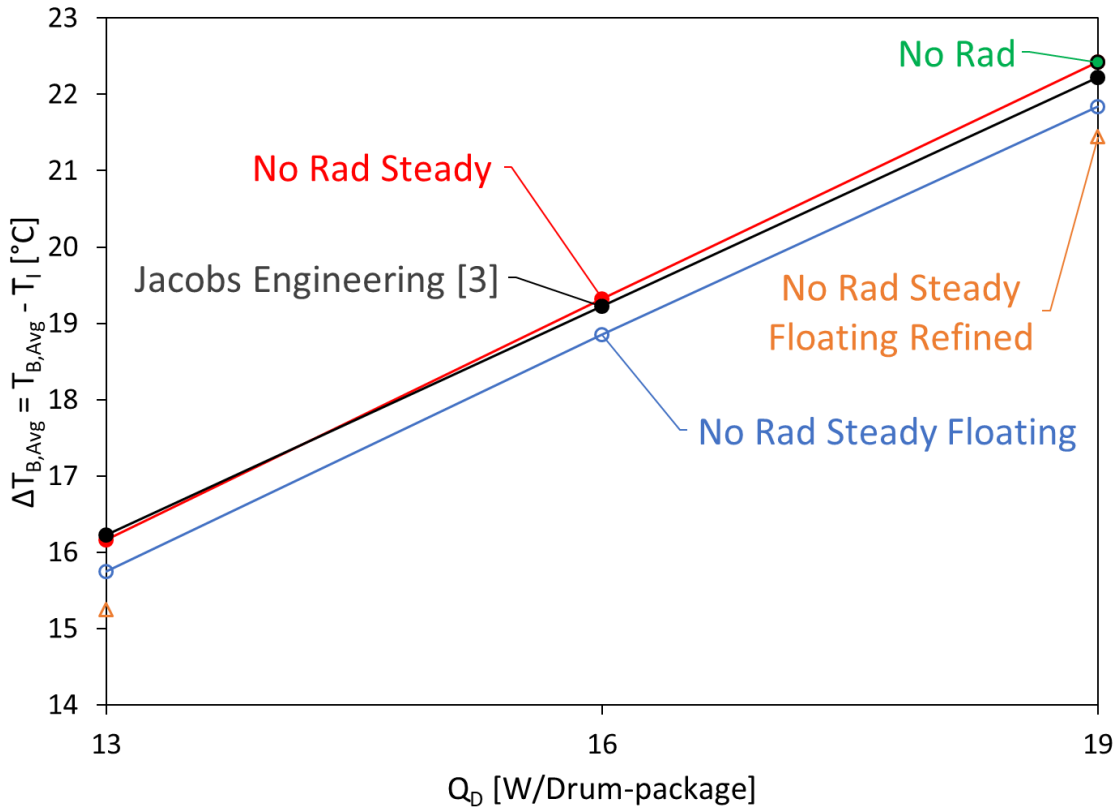

Figure 23: Difference between the average box-package surface temperature and inlet temperature versus drum-package heat generation rate. Results are shown from the current simulations that do not include radiation, and from Jacobs Engineering [3].

Jacobs Engineering did not specify if they included radiation heat transfer in their simulations. Figure 23 shows results for Conditions 5 through 8 which do not include radiation heat transfer, and Jacobs Engineering results. Figure 23 shows that excluding radiation heat transfer predicts average package surface temperatures that are roughly 1.5°C (2.7°F) warmer than when radiation heat transfer was included in Figure 22. Again, results from the transient and steady state rack simulations (Simulations 5-19W and 6-19W) are very similar to each other. Condition 6, No Rad Steady, gives temperatures that are roughly 0.6°C (1°F) warmer than Condition 7's, No Rad Steady Floating's, predictions. Condition 7 produced temperatures that are approximately 0.6°C (1°F) cooler than the Jacobs Engineering calculations. However, Condition 6's temperature predictions differ by

less than 0.3°C (0.5°F) from Jacobs Engineering's calculations. These results suggest that Jacobs Engineering may have excluded radiation heat transfer in their simulations. Since including radiation heat transfer cools box-package surface temperatures by approximately 1.5°C (2.7°F), we include it in the remainder of our simulations.

3.1.4: Mesh Sensitivity

In Figure 23, Condition 8 shows results from a mesh sensitivity study for the No Rad Steady Floating condition for two heat generations, Q_D = 13 and 19W. Condition 8, No Rad Steady Floating Refined, used 3.2 times as many elements as the nominal mesh for Condition 7, No Rad Steady Floating. For both 13 and 19W, Condition 8 predicted an average box-package surface temperature that was 0.4°C (0.8°F) cooler than the nominal case (Condition 7). For the remainder of this work, due to the increase in computational cost with a more refined mesh, and slightly more conservative (higher) temperature predictions, we employ the nominal 1.93M element mesh. An in-depth mesh sensitivity study should be conducted before developing a final predictive model to ensure mesh independence.

3.1.5: System Energy Balance

Table 6 shows the current work's simulations conducted at Q_D = 19W for all 8 conditions, as well as Jacobs Engineering's 19W simulation. The grid-based total heat generation rate applied to the system is given as Q_G. This is the actual total heat generation rate applied to the system, when calculated by ANSYS/Fluent. The nominal total heat generation rate applied to the system is equal to the heat generated from the packages (640 x 19W) plus the heat generated from the lights (8 x 100W), which results

in a total of 12,960W. The percent difference between the grid-based total heat generation rate and the nominal total heat generation rate is given as $Q_{G,\%}$.

Table 6: The absolute difference between the 1st law based (Equation 1) and simulated return air temperature increase based on total heat generation for a drum-package heat generation of 19W.

Return Air Temperature Increase For 19W/Package Heat Generation					
Simulation	Grid-based Heat Generation Rate	Heat Percent Difference	1st law based temperature increase	Simulated Temperature Increase	Temperature Difference
	Q_G [W]	$Q_{G,\%}$	$\Delta T_{R,1L}$ [°C]	ΔT_R [°C]	$\lvert\Delta T_{R,1L} - \Delta T_R\rvert$ [°C]
1-19W	13,058	0.8%	16.5	16.3	0.2
2-19W	11,728	9.5%	14.9	16.4	1.5
3-19W	12,961	0.0%	16.4	16.0	0.4
4-19W	12,961	0.0%	16.4	15.9	0.5
5-19W	11,019	15.0%	14.0	16.3	2.4
6-19W	11,022	15.0%	14.0	16.3	2.3
7-19W	12,961	0.0%	16.4	15.8	0.6
8-19W	12,962	0.0%	16.4	16.0	0.5
JE-19W [3]	12,960	0.0%	16.4	16.4	0.0

Table 6 is meant to verify that energy is conserved throughout the room simulations. To do so, the simulated return air temperature increase ΔT_R (return air temperature T_R minus inlet air temperature T_I) is compared to its theoretical value $\Delta T_{R,1L}$ based on the first law of thermodynamics as [9]

$$\Delta T_{R,1L} = \frac{Q_G}{\dot{m}_R C_P}. \quad (2)$$

Table 6 reports the temperature results for the highest package heat generation rate of Q_P = 19W as it leads to the highest ΔT_R and should produce the largest variations. To find the theoretical value, the grid-based total heat generation within the entire room Q_G, average return mass flow rate $\dot{m}_R$, average room air temperature $\overline{T}_{Room}$, and average specific heat at constant pressure for air within the room C_P are required. For all conditions $\overline{T}_{Room}$ = 35

(95) ± 1.1°C (2°F), so a constant C_P = 1.006 kJ/kg*K can be used for all conditions. Additionally, $\dot{m}_R$ = 0.785 ± 0.002kg/s, so a constant $\dot{m}_R$ = 0.785 can be used. These are all that is required to calculate $\Delta T_{R,1L}$. Table 6 also shows the absolute difference between ΔT_R and $\Delta T_{R,1L}$, which should be zero if energy is conserved throughout the room simulations.

The maximum difference is equal to 2.4°C (4.3°F) for Simulation 5-19W, which implies energy is not conserved for this simulation. A look into why the grid generated a total heat generation rate that is different from what was expected by the user (nominal total heat generation) may result in an explanation for the lack of energy conservation. The largest heat generation percent differences occur for Simulations 5-19W and 6-19W, which are both rack-box-package models.

When applying a surface heat flux to the box-package surfaces, a constant user input value for all conditions was used. However, when calculating the total heat generation rate applied to the system, ANSYS/Fluent produced values that varied depending upon the condition. This may be due to slight variances between different model meshes, producing slightly different box-package surface areas, and thus slightly different package heat generations.

The largest variance in total heat generation can be seen for the rack-box-package models and may be due to the application of shell conduction in creating the thin walls of the racks. In the mesh generator, the rack walls are modeled as thin walls for meshing simplicity. In the solver, shell conduction takes the thickness specified and creates additional mesh elements equal to the wall thickness. This allows both normal and tangential conduction through the rack walls. In the creation of these additional elements, some of which are in contact with the box-package surface, the surface heat flux applied from the box-package to the racks may have been modified by ANSYS/Fluent. It is unclear

what is producing the differences, but it is primarily seen for conditions employing the rack-box-package model, and the differences go away when shell conduction is turned off for the rack-box-package model. The grid-based total heat generation rate needs to be further investigated and controlled in future simulations.

Since the largest variance in Q_G (Simulation 1-19W vs. Simulation 5-19W) did not yield different temperature values, we do not expect this to have a significant effect on temperature results.

3.1.6: Package-to-Package Comparison

In addition to comparing the average and maximum package temperatures from different simulations, it is beneficial to compare all 160 individual box-package temperatures.

3.1.6.1: Effects of Radiation Heat Transfer on Comparison with Previous Work

Figure 24 shows the average surface temperature minus the air inlet temperature, $\Delta T_{B,1\text{-}19W} = T_{B,1\text{-}19W} - T_I$, for all 160 box-packages calculated from the current work's most complete simulation, 1-19W, plotted against the temperature difference predicted for the same box-package from Jacobs Engineering's JE-19W simulation, $\Delta T_{B,JE\text{-}19W} = T_{B,JE\text{-}19W} - T_I$. The line $\Delta T_{B,1\text{-}19W} = \Delta T_{B,JE\text{-}19W}$ is included in the plot. If the two simulations predicted the exact same box-package temperatures, then all data would lay on that line.

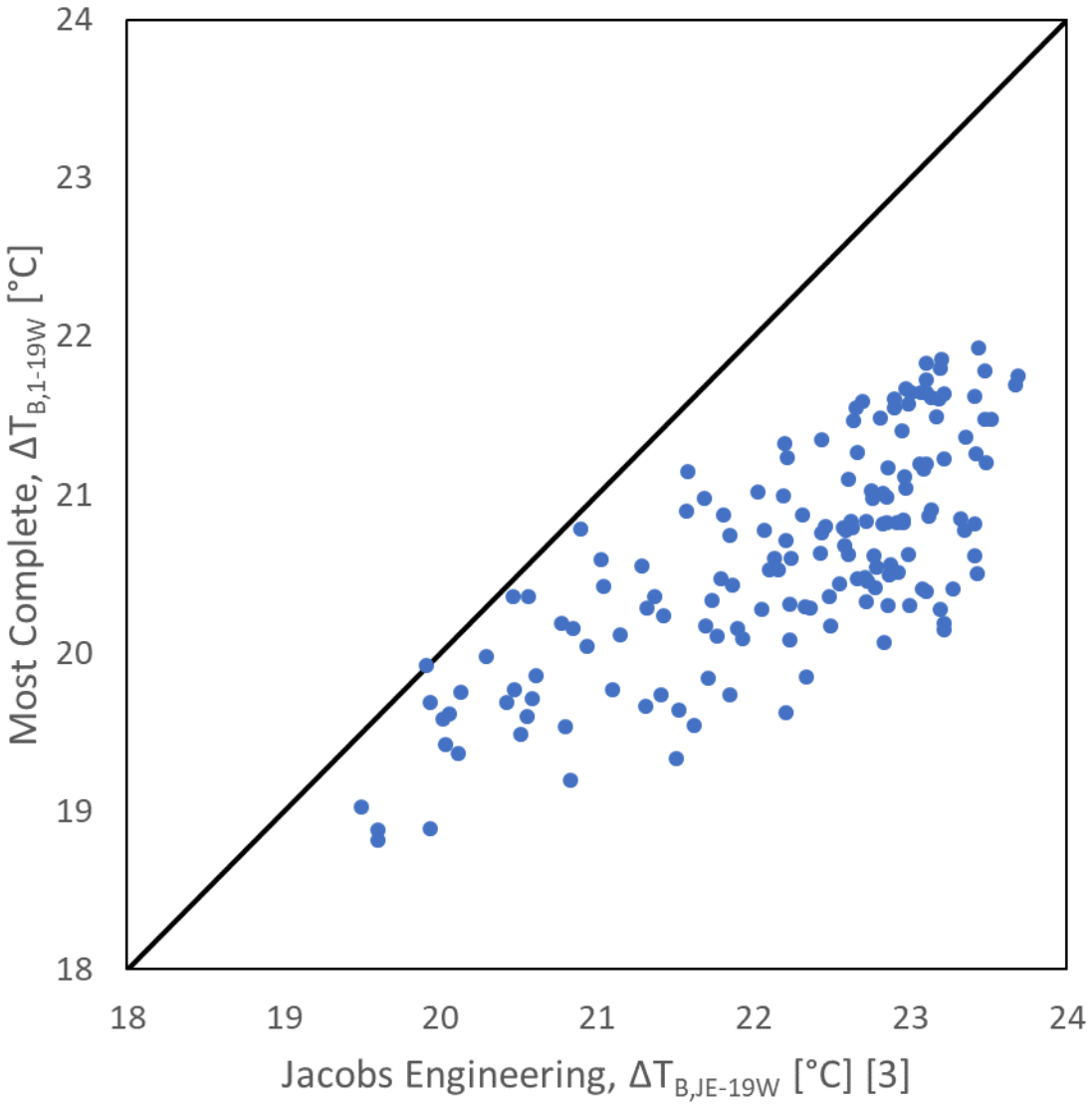

Figure 24: Individual box-package surface temperature for Simulation 1-19W versus JE-19W.

Figure 24 shows that while the temperatures predicted by Simulation 1-19W generally increase as the predictions from JE-19W increase, the data exhibits a random scatter. This indicates that there is not an exact correlation between the predictions, and suggests some random differences exist between the models constructed for this work and by Jacobs Engineering. Figure 24 also shows that Simulation 1-19W predicts individual box-package surface temperatures that are systematically cooler than those

predicted by the JE-19W simulation, as most of the data is below the $\Delta T_{B,1\text{-}19W} = \Delta T_{B,JE\text{-}19W}$ line. This, along with the earlier observation that Simulation 1-19W predicted lower average and maximum box-package surface temperatures than JE-19W, supports the notion that Jacobs Engineering may not have included radiation heat transfer.

Figure 25 is a plot of the temperature differences predicted by Simulation 5-19W (which is the most complete simulation from the current work that does not include radiation heat transfer) versus the temperature differences from Simulation JE-19W. Comparing Figure 24 and Figure 25 shows that in general, temperature predictions for Simulation 5-19W are systematically closer to Simulation JE-19W's predictions than were Simulation 1-19W's predictions. However, the data's random scatter appears slightly higher than in the previous case. We conclude that not including radiation heat transfer produces a prediction systematically closer to Jacobs Engineering, but possibly with a larger random scatter in individual box-package surface temperatures.

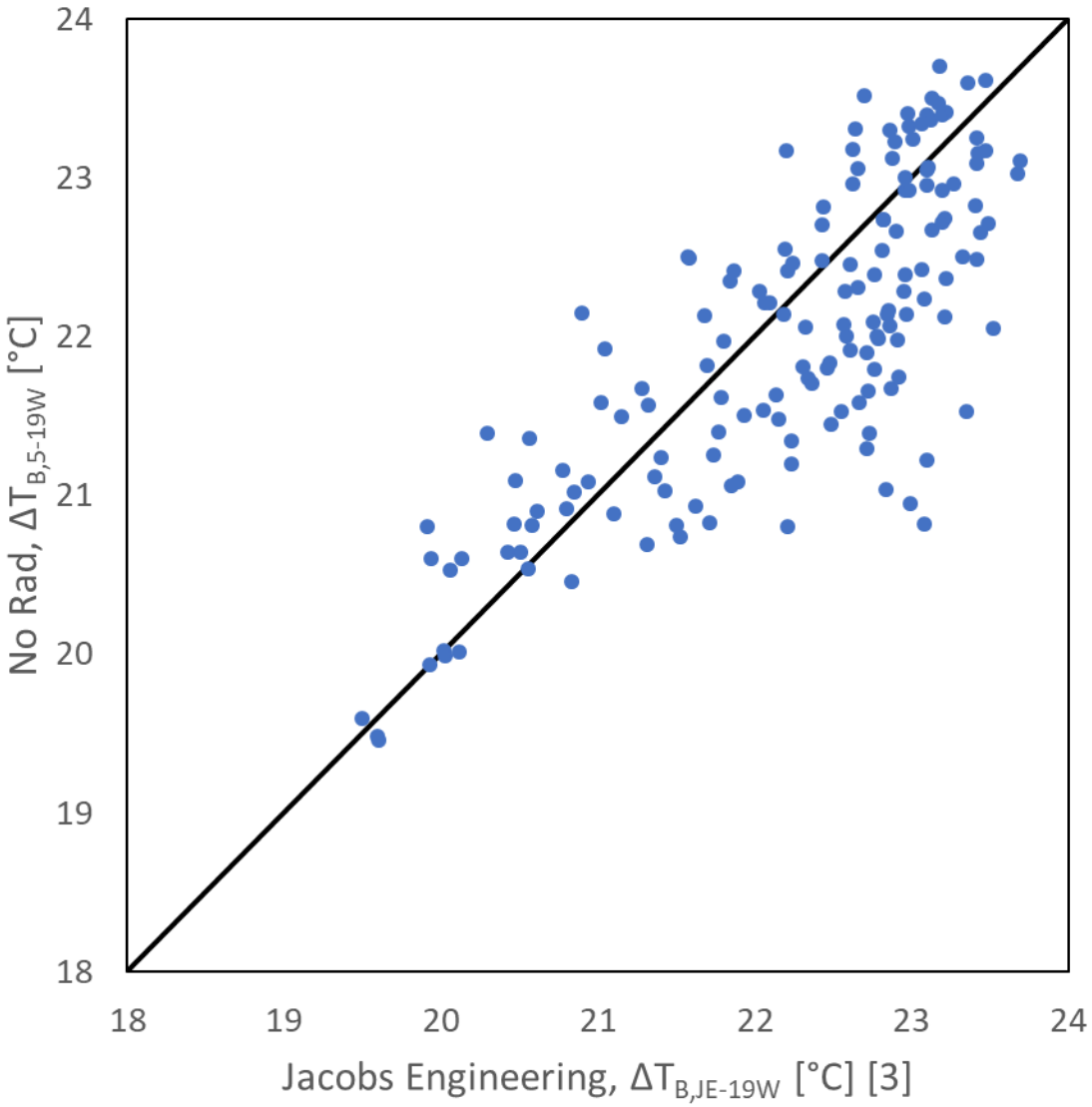

Figure 25: Individual box-package surface temperature for Simulation 5-19W versus JE-19W.

3.1.6.2: Comparison of Simulations from the Current Work

In this section, we compare results from different simulations performed in the current work. Because different simulations include different physical phenomena, and employ different models, we expect that they will not predict identical results. We wish to quantify the differences between the results for different simulations. We will use these results to rationally select methods to employ in predictive models.

Figure 26 shows temperature differences predicted by Simulation 2-19W (Steady) versus those predicted by Simulation 1-19W (Most Complete); the dotted line is fit to the data. The two-standard error of the estimate, $\sigma_{95\%}$, quantifies the average deviation above and below the best fit line that includes 95% of the data [10]. It is calculated as

$$\sigma_{95\%} = 2\sqrt{\frac{\sum(\Delta T_B - \Delta T_B{}')^2}{N-2}}. \quad (3)$$

In this expression, ΔT_B is the individual box-package's average surface temperature minus the room inlet temperature, ΔT_B' is the predicted value based on the linear regression of the data, and N = 160 is the number of box-packages.

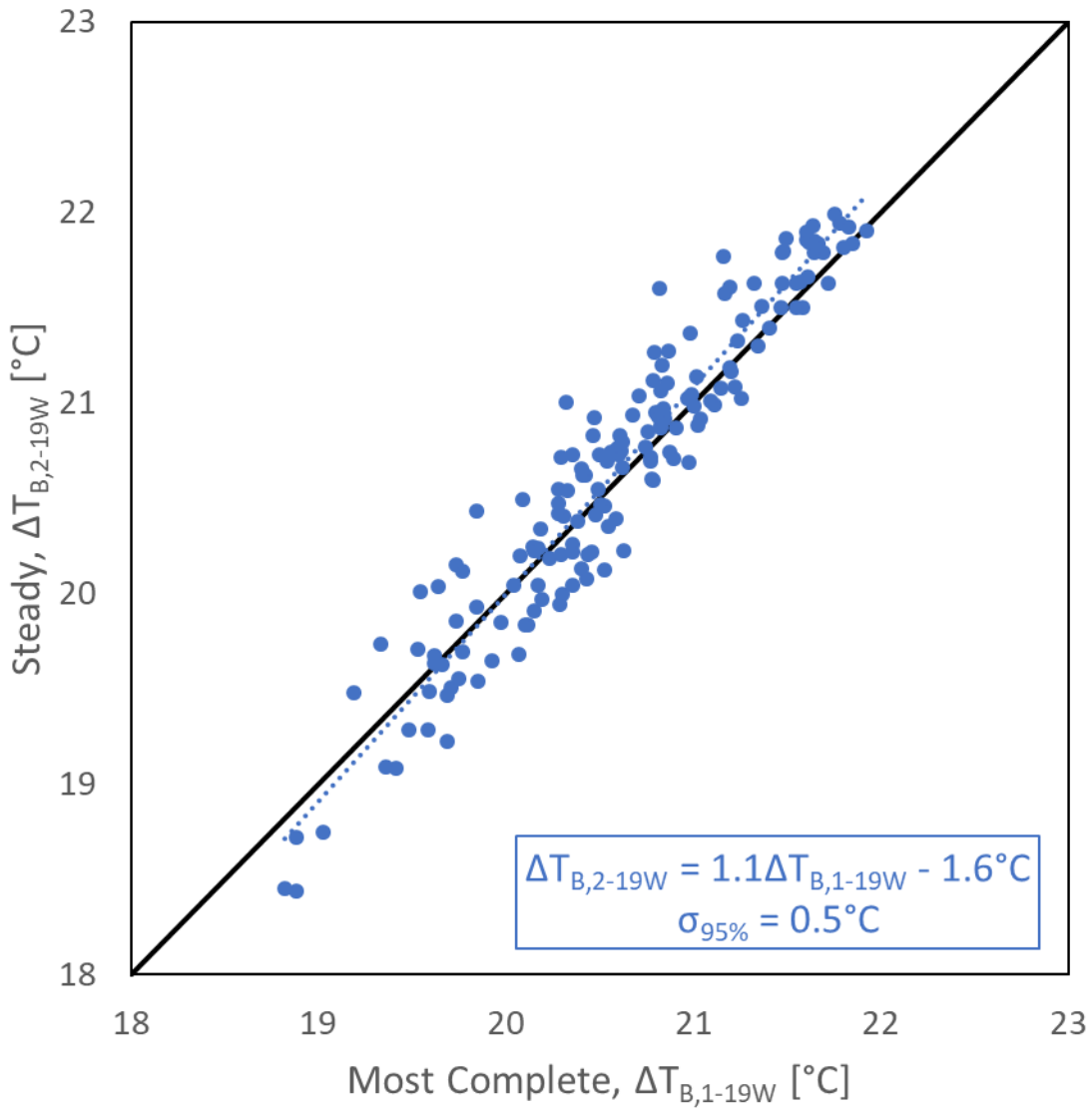

Figure 26: Individual box-package surface temperature for Simulation 2-19W versus Simulation 1-19W.

The equation of the best fit line and the two-standard error value are given in the figure. The two-standard error value indicates that 95% of the temperature differences predicted by Simulation 2-19W, Steady, are within 0.5°C (0.9°F) of the best fit line. Comparison of the dotted and solid lines in Figure 26 shows that, on average, Simulation 2-19W predicts slightly higher temperatures for the warmer packages than Simulation 1-19W, and slightly lower temperatures for the cooler ones. Overall, even though Simulation

2-19W does not include unsteadiness, its results are highly correlated with, and on average quite close to, the results of Simulation 1-19W. The latter simulation includes unsteadiness and requires far more computational resources. For this reason, steady state simulations are used for the remaining simulations in this work.

Figure 27 shows the package temperature difference from Simulation 3-19W (Steady Floating) versus 1-19W (Most Complete), with general temperature predictions for Simulation 3-19W lying very close to 1-19W's predictions, with $\sigma_{95\%}$ = 1.0°C (1.8°F). Comparison of the dotted and solid lines in Figure 27 shows that, on average, Simulation 3-19W predicts slightly lower temperatures than Simulation 1-19W, but with a smaller difference for the warmer packages. Overall, even though Simulation 3-19W does not include unsteadiness or racks, its results are highly correlated with, and on average quite close to, the results of Simulation 1-19W. Removing the racks does not significantly vary the systematic temperature predictions, only slightly increases the random scatter of the data, and reduces the computational resources required. For this reason, steady state floating simulations are used for the remaining simulations in this work.

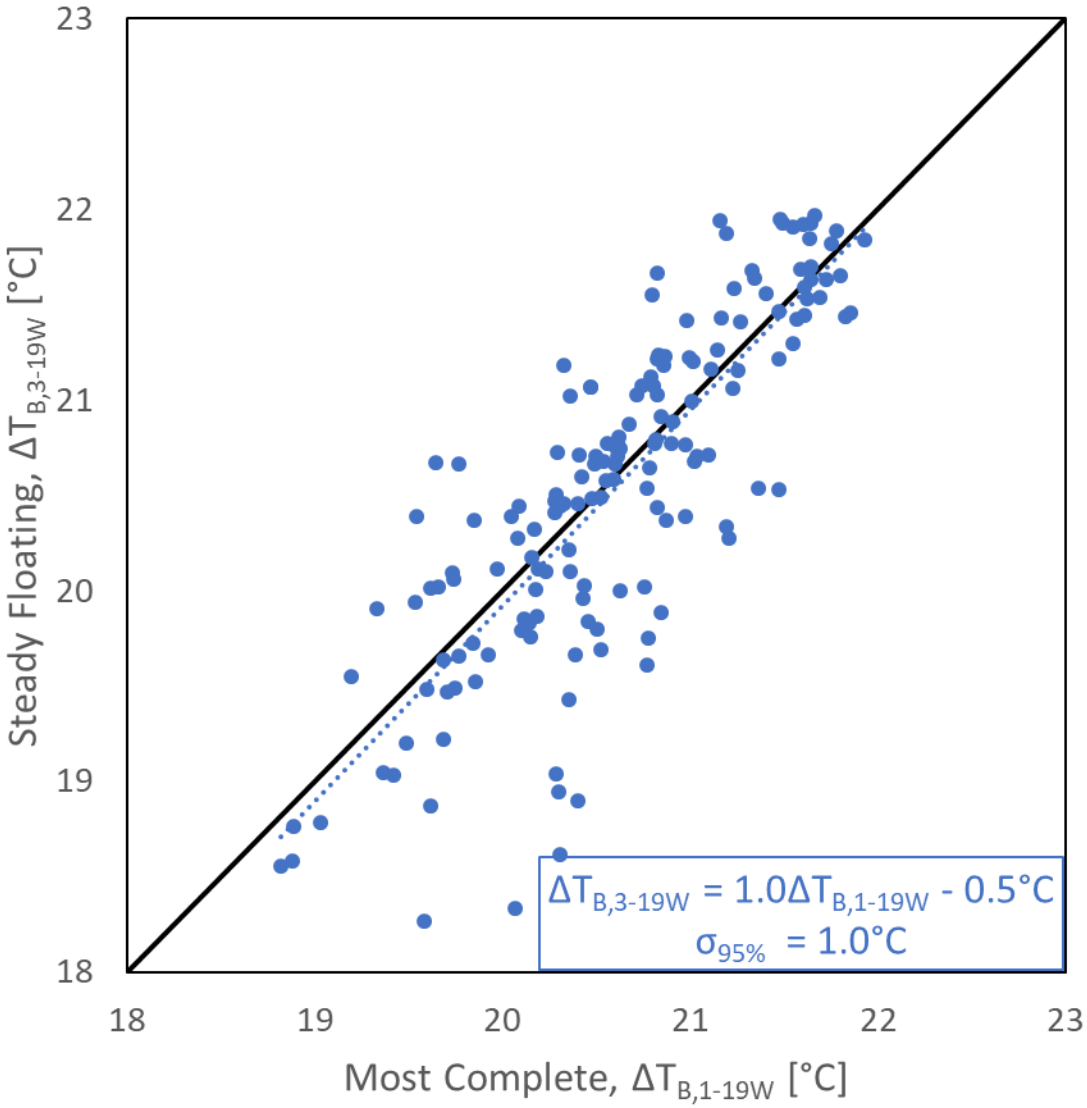

Figure 27: Individual box-package surface temperature for Simulation 3-19W versus Simulation 1-19W.

3.2: Drum-package Model

In the second stage, we investigate the effect of modeling individual drum-packages compared to box-packages by explicitly modeling the drum-packages and comparing differences in the results. This allows us to determine if the box-package model loses important details of the airflow and drum-package surface temperatures.

The Jacobs Engineering model grouped sets of four drum-packages as a single box-package [3]. While this reduced model complexity and resource cost, it neglects air flow around the individual drum-packages and reduces overall air flow through the rows. Box-packages also make it difficult to predict internal component temperatures and remove the possibility of varying individual drum-package heat generation rates.

In this section we simulate individual floating-drum-packages, without including the racks. Instead of modeling four drum-packages as one box-package, each drum-package is modeled as a simple cylindrical drum, and the total heat dissipated by each drum-package is equal to Q_D. There are 640 drum-packages grouped into the 160 bay locations in the room. Based on the close correlation and good agreement between the results of the transient rack-box-package simulations and steady state floating-box-package simulations described in the last section, we performed steady state simulations of the floating-drum-package model, with radiation heat transfer.

3.2.1: Drum-package Model Airflow Variations

All the tables and figures presented in this section follow the same format as the tables and figures presented in the box-package model section to provide a more direct comparison between the two models.

Figure 28 shows a full isometric view of the temperature contours of the drum-package surfaces. Like Figure 16, the surface temperatures are nearly uniform and the drum-packages close to the ceiling and door wall are somewhat cooler than the rest due to their proximity to the HVAC air diffusers and return ducting.

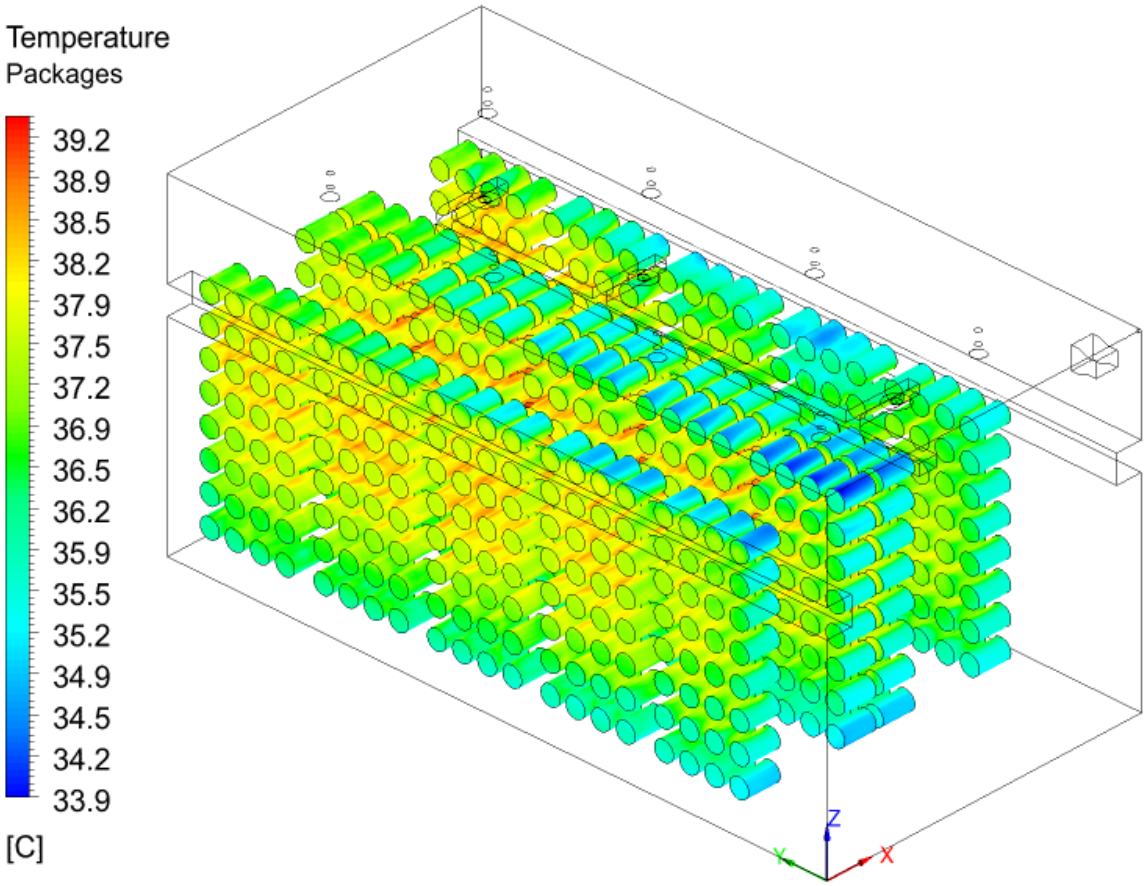

Figure 28: Floating-drum-package with radiation heat transfer full isometric view.

Figure 28 also shows that the upper surfaces of some of the drum-packages near the mid-height are warmer than most surfaces. Figure 29 shows the same temperature contour data as Figure 28, but with the first two rows removed to show the warmer regions. Like Figure 17, it shows that the side and top drum-package surfaces near the mid-height of the rows exhibit the highest temperatures.

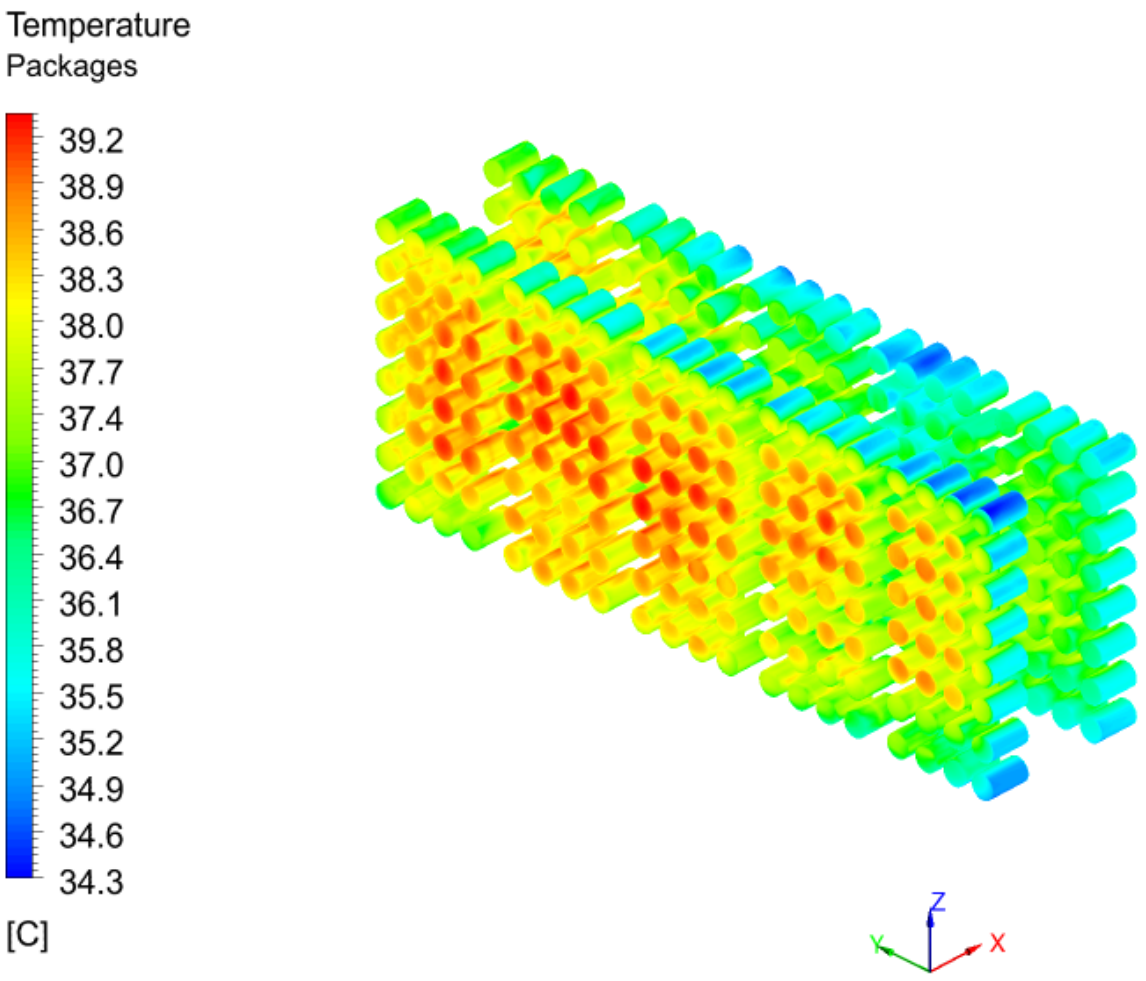

Figure 29: Floating-drum-package with radiation heat transfer half isometric view.

Figure 30 shows the airflow pattern and temperature contours in a plane in the middle of the first aisle, at x = 2.6m (8ft 7in). The velocity vectors shown are the tangential components of the air velocity in that plane, with the length of the vectors representing a range from 0-0.6m/s. Instead of one large recirculating flow eddy, as was the case in the rack-box-package model shown in Figure 18, the air has a more upward flow in the aisle. There is still a significant downdraft of cool air along the door wall. The additional regions of air in between the individual drum-packages results in more flow throughout the drum-package region of the room and upward flow in the aisle.

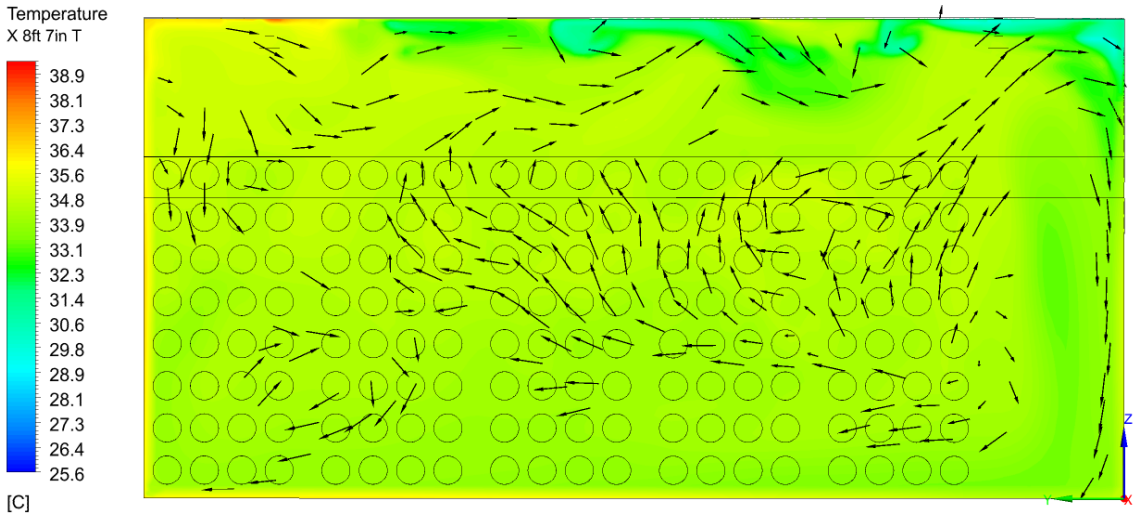

Figure 30: Floating-drum-package with radiation heat transfer first aisle, x = 2.6m (8ft 7in).

Figure 31 shows the airflow pattern and temperature in the middle of the third row, at x = 5.1m (16ft 10in). This row was selected because it contains the hottest drum-package. The velocity vectors shown are the tangential components of the air velocity in that plane, with the length of the vectors representing a range from 0-1.1m/s. Here, instead of the air being blocked vertically between different elevations of box-packages, air can flow more freely around the drum-packages increasing the convective heat transfer around the drums.

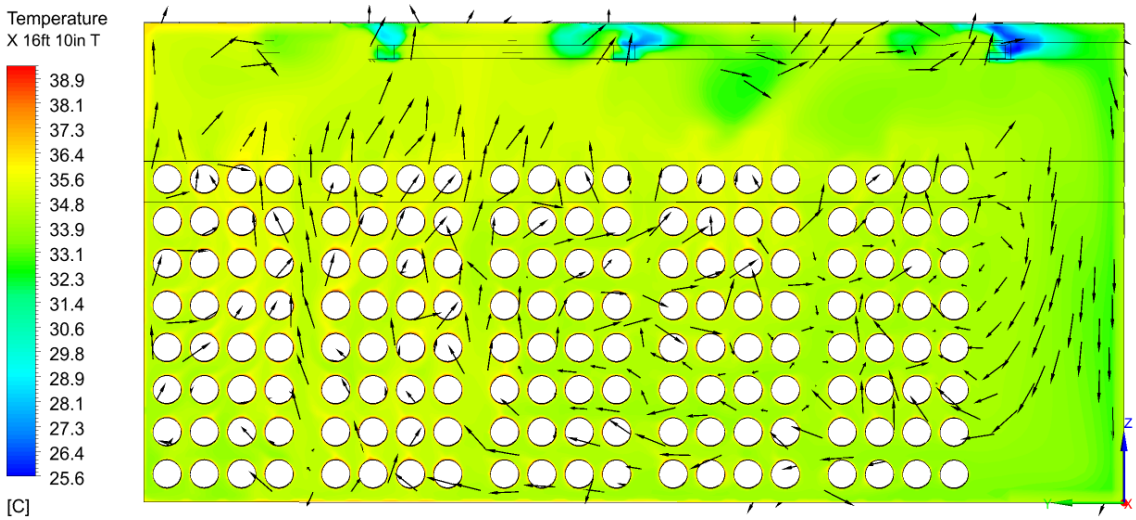

Figure 31: Floating-drum-package with radiation heat transfer third row, x = 5.1m (16ft 10in).

Figure 32 shows the airflow pattern and temperature in the mid-height of the room, at z = 4.5m (14ft 9in). The velocity vectors shown are the tangential components of the air velocity, with the length of the vectors representing a range from 0-0.6m/s. The air flows in between the drum-packages, instead of only flowing toward the door along the aisles as was the case with the rack-box-package model in Figure 21. The increased infiltration of air around the drum-packages allows for increased cooling of the drum-packages, which is reflected by the drum-package surface temperature results.

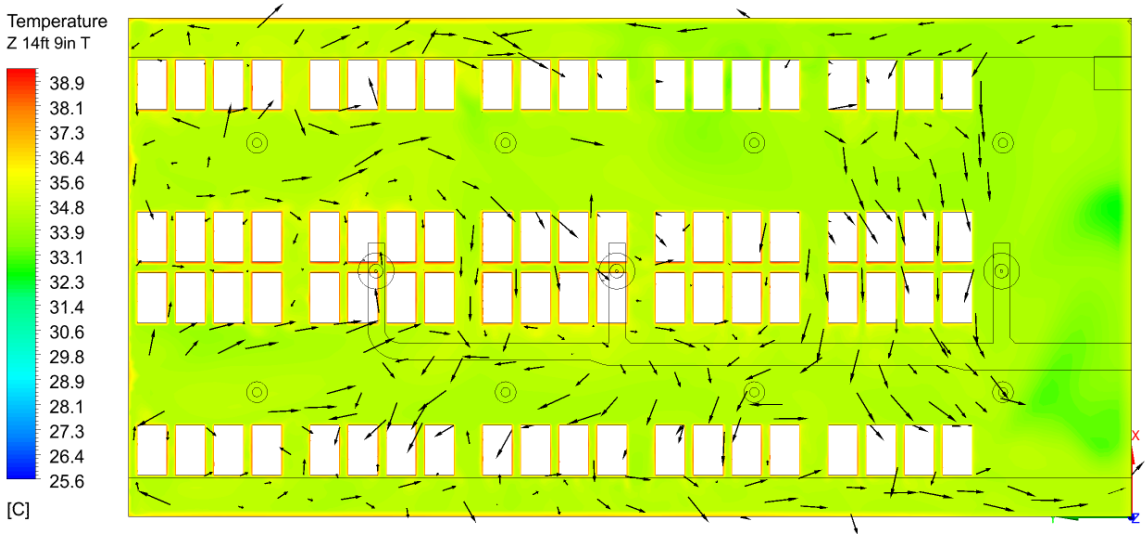

Figure 32: Floating-drum-package with radiation heat transfer mid-height, z = 4.5m (14ft 9in).

3.2.2: Model Variations Summary

Table 7 summarizes the current work's 3 drum-package conditions performed. Condition 9 includes radiation heat transfer with a surface emissivity throughout the room of $\epsilon = 1$. Condition 10 includes radiation heat transfer with the 9975 package's external surface emissivity ($\epsilon = 0.21$) applied to the drum-package surfaces, and a surface emissivity of $\epsilon = 1$ everywhere else [2]. Condition 11 does not include radiation heat transfer. It should be noted that all conditions were steady state without racks, and they

employed the SST k-ω turbulence model. A total of 7 simulations were conducted with Q_D = 13, 16, or 19W.

Table 7: Summary of all 7 drum-package simulations performed in this work.

Condition Number	Condition Name	Time Dependence	Radiation Heat Transfer	Racks	Mesh	Turbulence Model	Q_D [W]
Current Work							
9	Drum, ϵ = 1	Steady	Yes, ϵ = 1	No	9.0E+06	SST k-ω	13, 16, 19
10	Drum, ϵ = 0.21		Yes, ϵ = 0.21				19
11	Drum, No Rad		No				13, 16, 19

Table 8 summarizes the results from the current work for the drum-package model. For each simulation, the heat generation rate Q_D is given, which is equivalent to one drum-package's heat generation rate. The location of the hottest drum-package, $\Delta T_{D,Max}$, and $\Delta T_{D,Avg}$ are also provided.

Table 8: The location and temperature of the hottest drum-package for current work. The average drum-package temperature and resource cost is also included.

Condition Number	Q_D [W]	Location of hottest drum-package				$\Delta T_{D,Max}$ [C]	$\Delta T_{D,Avg}$ [C]	RC [Core-hr]	Operating System
		Rack	Bay	Drum	Elevation				
9	19	3	4	3	5	20.7	19.6	4,200	Linux (80 Cores)
	16	3	4	3	5	17.9	16.9		
	13	3	4	3	5	14.9	14.1		
10	19	3	5	4	6	21.0	20.1	4,500	Linux (120 Cores)
11	19	2	5	4	6	22.0	20.7	1,400	Linux (80 Cores)
	16	2	5	4	6	19.0	17.9		
	13	2	5	4	6	15.9	15.0		

Table 8 shows that the location of the hottest drum-package varies depending on the simulation. The rectangular prism region between Rack 2, Bay 4, Drum 3, Elevation 5

and Rack 3, Bay 5, Drum 4, Elevation 6 represents the hottest region regardless of the condition or package heat generation. The hottest drum-package is at most 1.3°C (2.3°F) warmer than the average drum-package surface temperature, occurring for Simulation 11-19W.

Table 8 also summarizes the resource cost required for all drum-package conditions. Floating-drum-package Conditions 9 and 11 are only 83% less computationally expensive when compared to the rack-box-package Conditions 2 and 6 in Table 4. The floating-drum-package Conditions 9 and 11 are 3.3 times more computationally expensive when compared to the floating-box-package Conditions 3 and 7 in Table 4 due to a higher mesh count. The floating-drum-package model is more computationally expensive compared to the floating-box-package model. However, the changes in both temperature and airflow results may be large enough to warrant the use of a drum-package model in the final predictive model.

3.2.3: Global Results

Figure 33 shows $\Delta T_{D,Avg}$ versus Q_D for all conditions listed in Table 7, as well as box-package Conditions 3 and 7. Conditions 3 and 9 include radiation heat transfer with a surface emissivity $\epsilon = 1$ and are shown with square symbols. Simulation 10-19W includes radiation heat transfer with a drum-package surface emissivity $\epsilon = 0.21$ and is shown with an X symbol. Conditions 7 and 11 do not include radiation heat transfer and are shown with circular symbols.

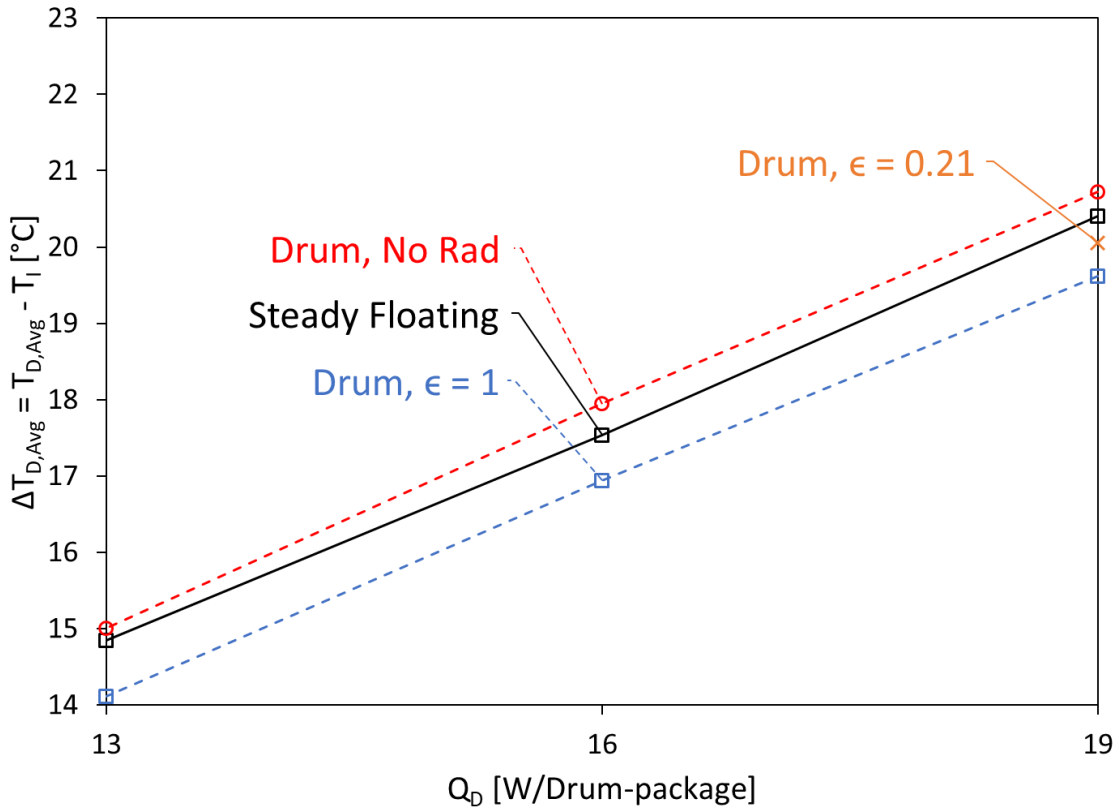

Figure 33: Difference between the average drum-package surface temperature and room inlet temperature versus package heat generation rate. All the current simulation results in this plot are for the drum-package model. Results from Jacobs Engineering are also included [3].

For Condition 10, a package heat generation rate of 19W was the only simulation conducted as it is expected that the lower heat generation results for this condition would be bounded by Conditions 9 and 11, as is the case for Simulation 10-19W.

The drum-package model predicted that average drum-package surface temperatures for Conditions 9 and 11 were at most 1.1°C (2°F) cooler than their similar box-package Conditions 3 and 7, respectively. This may be due to the increased airflow around the individual drum-packages. No Rad Drum, Condition 11, has a higher mesh count than No Rad Steady Floating, Condition 7. Also, No Rad Steady Floating Refined (Condition 8) predicted an average box-package surface temperature which was 0.4°C

(0.8°F) cooler than the nominal case (Condition 7). Condition 10 is only 0.5°C (0.9°F) cooler than Condition 8.

Simulation 10-19W predicted an average drum-package surface temperature 0.5°C (0.9°F) warmer than simulation 9-19W, due to the change in drum-package surface emissivity. This is to be expected as simulation 10-19W models less efficient radiation heat transfer when compared to simulation 9-19W. A final predictive model should use the proper emissivity value of all surfaces in the room.

Chapter 4: Summary, Conclusions and Future Work

4.1: Summary

Radiological materials that are actively generating heat are contained within drum-style packages for shipping and staging purposes. These drum-packages must be designed to contain the materials and shield the surroundings. To do so, the drum-packages have various components which must not exceed specified temperature limits. These drum-packages have been tested and certified under specific Normal Conditions of Transport (NCT). Their contents must not exceed a heat generation rate of 19W. It may be beneficial to stage multiple drum-packages in a high-density staging configuration, where they can be stacked on a racking system inside a room. To do so, a CFD based model that can predict the radiological package temperatures may be useful. In previous work, Jacobs Engineering modeled 640 drum-packages in a generic staging facility which was roughly 18.3m long x 9.1m wide x 9.1m tall (60ft x 30ft x 30ft) [3]. Their model included adiabatic walls, 8 ceiling lights generating 100W each (800W total), and an extensive racking system for the packages to sit on. An HVAC system included supply ducting near the ceiling which provided 0.78 kg/s (1370 ACFM) of air at 17.8°C (64°F) and allowed air to freely return through one return duct. For model simplification, Jacobs Engineering modeled four drum-packages lying on their sides as a single rectangular prism box-package. This created 160 box-packages arranged into four racks, five bays within each rack, and eight vertical elevations. Simulations were conducted for individual drum-package heat generation rates of 13, 16, and 19W. The current work begins by reproducing the Jacobs Engineering model results with a highly detailed room model

which includes a racking system, box-packages, and radiation heat transfer conducted as a transient simulation. The current work also performed a scoping study to determine the effects of various model components on the drum-package temperature results. These components include time dependence, geometry, turbulence model employed, radiation heat transfer, and drum-package or box-package modeling.

4.2: Conclusions

While all the model components affected the surface temperatures of radiological packages within a generic staging building, some simplifications can be made when creating a final predictive model.

First, steady state simulations appear to provide a close approximation to transient simulations and can be used as they are 7.8 times more computationally efficient than transient simulations. Second, the SST k-ω turbulence model has been used in previous studies and is found to be more conservative than the RNG k-ε turbulence model in the current work. Third, a nominal mesh size of 1.93E6 elements maximizes computational efficiency without changing package surface temperature predictions by more than 0.4°C (0.7°F). However, a thorough mesh independence study should be done on the final predictive model. Fourth, a floating package model is not as geometrically accurate as the rack model but requires roughly 1/4 of the computational resources. Lastly, Floating-drum-packages may model airflow more accurately, will allow individual package heat generation rates to be specified, and can provide individual drum-package component temperatures, however, they require roughly 3 times more computational resources than floating-box-packages. Some of these simplifications affect the results and computational resource cost more significantly than others. While the current work provides a wide array

of model comparisons, when choosing a final predictive model, additional studies will be required.

4.3: Future Work

The current work is meant to establish a complete scoping study for a generic radiological package staging building, so that a predictive model can then be used to determine a compact staging configuration that will not allow package surface temperatures to exceed their safety limit.

If the floating-drum-package model is found to be the final predictive model, a rack-drum-package model study could be conducted as the surface area of the drum-packages in contact with the racks is significantly smaller and may produce different conclusions than the rack-box-package models.

To determine the final predictive model, it could be determined what would be beneficial to include in the model, as well as what is desired from the model. For example, it may be beneficial to allow multiple room geometries with a variable number of packages and drum-package heat generation rates. It may also be beneficial to apply different HVAC parameters or include heat dissipation through the walls to simulate poorly insulated walls. It may be desirable to have the model determine location and temperature of the hottest packages and determine if any temperature limits have been exceeded.

The package which has the maximum average surface temperature could be further investigated to verify internal component temperature limits are not exceeded. Since the internal components are not modeled in the current work, the internal component temperatures are unknown.

It may be beneficial to conduct a transient simulation which includes a loss of power to the HVAC system for a certain period of time, after which the HVAC system starts

back up. The package temperatures could be monitored until the room returns to a quasi-steady state to determine if this temporary disruption risks exceeding package temperature safety limits.

As this work found difficulty in controlling the total package heat generation rate with an applied surface heat flux, the effects of this could be determined and the package heat generation rate could be controlled.

Future work could include radiation heat transfer with a package surface emissivity of $\epsilon = 0.21$, as the current work's use of $\epsilon = 1$ or exclusion of radiation heat transfer was performed to reproduce Jacobs Engineering's results.

Upon confidence of a specific ANSYS/Fluent model, a graphical user interface or excel interface could be developed to allow for the use by engineers with limited CFD experience. This interface could allow one to select the number and location of packages, as well as their individual heat generation rate. The model could be able to determine if the specified condition results in any package temperatures exceeding their temperature limits.

Appendix A: Governing Equations

The flow of the system is modeled as incompressible flow, and the density of the fluid within the system can be found as

$$\rho = \frac{P_{OP}}{\frac{R}{M_W}T}. \quad (4)$$

The operating pressure of the system, P_{OP}, is equal to 101.325 kPa [8]. The universal gas constant, R, is equal to 8.314 kJ/(kmol*K) [9]. The molecular weight of air, M_W, is 28.97 kg/kmol [9]. Temperature is calculated by ANSYS/Fluent.

The equation for conservation of mass throughout the system is

$$\frac{\partial \rho}{\partial t} + \nabla \cdot (\rho \vec{v}) = S_m. \quad (5)$$

S_m is the mass added to the system within the domain, and is equal to 0 in our case [11].

The equation for conservation of momentum throughout the system is [11]

$$\frac{\partial}{\partial t}(\rho \vec{v}) + \nabla \cdot (\rho \vec{v}\vec{v}) = -\nabla \mathrm{P} + \nabla \cdot (\bar{\bar{\tau}}) + \rho \vec{g} + \vec{F}. \quad (6)$$

P is the static pressure of the system, $\rho \vec{g}$ is the gravitational force, $\vec{F}$ is additional external forces, and $\bar{\bar{\tau}}$ is the stress tensor given by

$$\bar{\bar{\tau}} = \mu[(\nabla \vec{v} + \nabla \vec{v}^T) - \frac{2}{3}\nabla \cdot \vec{v} I]. \quad (7)$$

μ is the molecular viscosity, and I is the unit tensor [11].

The equation for conservation of energy throughout the system is

$$\frac{\partial}{\partial t}(\rho E) + \nabla \cdot \left(\vec{v}(\rho E + P)\right) = \nabla \cdot \left(k_{eff} \nabla \mathrm{T} - \sum_j h_j \vec{J}_j + \left(\bar{\bar{\tau}}_{eff} \cdot \vec{v}\right)\right) + S_h. \quad (8)$$

k_{eff} is the effective thermal conductivity, $\vec{J}_j$ is the diffusion flux of each species j, and S_h is heat added to the system within the model [11].

References

[1] "10 CFR Part 71 - Packaging and Transportation of Radioactive Material," *Nuclear Regulatory Commission*, Sep. 2020.

[2] Savannah River National Laboratory, "Safety Analysis Report Model 9975." Savannah River Nuclear Solutions, LLC, Apr. 2014.

[3] Austin Flynt, "ESP-491 HVAC CFD Modeling: Phase 2 CFD Report." Jacobs Engineering, Mar. 10, 2020.

[4] A. Hellsten, "Some improvements in Menter's k-omega SST turbulence model," in *29th AIAA, Fluid Dynamics Conference*, American Institute of Aeronautics and Astronautics, 1998.

[5] C. Porras-Amores, F. R. Mazarrón, and I. Cañas, "Study of the Vertical Distribution of Air Temperature in Warehouses," *Energies*, vol. 7, no. 3, Art. no. 3, Mar. 2014.

[6] L. L. Wang and W. Li, "A study of thermal destratification for large warehouse energy savings," *Energy Build.*, vol. 153, pp. 126–135, Oct. 2017.

[7] Z. Zhang, Z. (John) Zhai, W. Zhang, and Q. (Yan) Chen, "Evaluation of Various Turbulence Models in Predicting Airflow and Turbulence in Enclosed Environments by CFD: Part 2-Comparison with Experimental Data from Literature," *HVACR Res.*, vol. 13, no. 6, pp. 871–886, Nov. 2007.

[8] "ANSYS FLUENT 12.0 User's Guide." .

[9] Y. A. Cengel and M. A. Boles, *Thermodynamics: An Engineering Approach*, 8th ed. McGraw-Hill, 2015.

[10] David Lane, *Introductory Statistics*. LibreTexts, 2021.

[11] "ANSYS FLUENT 12.0 Theory Guide." .